Article:
Ward, S.L., Bradley, S.L., Wilmes, S. et al. (2026) Relative sea-level change, tidal evolution and energy dissipation across the Patagonian shelf since the last glacial maximum. Paleoceanography and Paleoclimatology, 41 (5). e2025PA005384. ISSN: 2572-4517

https://doi.org/10.1029/2025pa005384

Paleoceanography and Paleoclimatology

RESEARCH ARTICLE
10.1029/2025PA005384

Key Points:

- We present the first regional paleotidal reconstruction for the Patagonian Shelf, for the Last Glacial Maximum to present day
- Sea-level and coastline changes over the last 21,000 years have driven major non-linear responses in tidal dynamics across the shelf
- Model outputs support research on sea-level indicators, biogeographic connectivity, and long-term carbon accumulation

Supporting Information:

Supporting Information may be found in the online version of this article.

Correspondence to:

S. L. Ward,
sophie.ward@bangor.ac.uk

Citation:

Ward, S. L., Bradley, S. L., Wilmes, S.-B., Roseby, Z. A., Green, J. A. M., Robins, P. E., et al. (2026). Relative sea-level change, tidal evolution and energy dissipation across the Patagonian Shelf since the Last Glacial Maximum. *Paleoceanography and Paleoclimatology*, *41*, e2025PA005384. https://doi.org/10.1029/2025PA005384

Received 1 DEC 2025
Accepted 28 APR 2026

Author Contributions:

Conceptualization: S. L. Ward, J. D. Scourse
Data curation: S. L. Ward, S. L. Bradley, S-B. Wilmes
Formal analysis: S. L. Ward, S. L. Bradley, S-B. Wilmes
Funding acquisition: C. M. Roberts
Investigation: S. L. Ward, S. L. Bradley, S-B. Wilmes, Z. A. Roseby
Methodology: S. L. Ward, S. L. Bradley, S-B. Wilmes, Z. A. Roseby, J. A. M. Green, P. E. Robins
Project administration: J. D. Scourse
Supervision: J. D. Scourse
Validation: S. L. Ward, S. L. Bradley, S-B. Wilmes

Relative Sea-Level Change, Tidal Evolution and Energy Dissipation Across the Patagonian Shelf Since the Last Glacial Maximum

S. L. Ward[1], S. L. Bradley[2], S-B. Wilmes[1], Z. A. Roseby[3], J. A. M. Green[1], P. E. Robins[1], C. M. Roberts[4], and J. D. Scourse[3]

[1]School of Ocean Sciences, Bangor University, Menai Bridge, UK, [2]School of Geography and Planning, University of Sheffield, Sheffield, UK, [3]Department of Earth and Environmental Sciences, University of Exeter, Cornwall, UK, [4]Centre for Ecology and Conservation, University of Exeter, Cornwall, UK

Abstract Tides play a key role in regulating shelf-sea environments, influencing sediment dynamics, habitat distribution, long-term carbon burial, coastal hazards, and water quality, with important socio-economic consequences. Yet the long-term evolution of shelf sea tides in response to sea-level change remains poorly understood. We have developed the first regional paleotidal reconstruction for the Patagonian Shelf, one of the most tidally energetic regions globally, supporting high primary productivity and sustaining rich food webs. The model incorporates updated relative sea-level reconstructions and is driven by global paleo-ocean forcing. Tidally modulated parameters are produced at 1,000-year intervals from the Last Glacial Maximum (21,000 years ago) to the present. The reconstruction shows how tidal dynamics across the shelf are sensitive to relative sea-level change. Overall, present-day tidal dynamics are relatively energetic compared with much of the deglacial period. Tidal energy dissipation responded non-linearly to shelf inundation, with changes in coastline configuration and water depth driving abrupt reorganizations of regional tidal dynamics and associated frictional hotspots. The M_2 tidal energy dissipation dominated throughout, peaking at 10 ka BP (+16% relative to present-day). Dissipation for O_1 was highly sensitive to shelf evolution, peaking at ~50% above present-day at 15 ka BP. This work establishes a baseline for future interdisciplinary studies, providing open-access simulations that improve interpretation of sea-level indicators, long-term coastal evolution, environmental archives, and seabed management across the Patagonian Shelf.

Plain Language Summary Tides play a key role in shaping coastal environments, influencing water quality, affecting flooding, transporting sediments, carbon and nutrients, and driving physical processes that underpin marine habitats and ecosystems. Today, the Patagonian Shelf is one of the world's most tidally-energetic regions, but little is known about how these tides changed as sea levels rose after the last ice age. This study explores how tides evolved across the Patagonian Shelf over the last 21,000 years. Using new sea-level reconstructions of the shelf, we developed the first high-resolution simulations of past tides for the region, revealing how past changes in water depth and shelf shape influenced tidal dynamics through time. Our results reveal that modern tides across the shelf are among the strongest in the last 21,000 years. We show that the tides are sensitive to even modest late-glacial and Holocene fluctuations in sea levels, which is an important consideration for how the tides across the shelf could respond to future sea-level rise. All model outputs and derived data sets are openly available to support future work on past environments, archeology, sea-level reconstructions, ecosystem change, and sedimentary blue carbon.

1. Introduction

Continental shelf seas are a key component of the Earth system, with their evolving form and function shaping major ocean and climate processes over geological time. Tides are a major driver of physical and ecological processes across global shelf seas, influencing short-term responses such as energy dissipation and flooding (e.g., Egbert & Ray, 2001; Pugh & Woodworth, 2014), and longer-term processes such as seasonal stratification, morphodynamics, and carbon accumulation (e.g., Hinton, 1996; Rippeth et al., 2008; Scourse et al., 2002; Ward, Bradley, Roseby, et al., 2025). During the global Last Glacial Maximum (LGM; 26.5–19 ka; Clark et al., 2009), global mean sea level (or barystatic sea level, Gregory et al. (2019)) was approximately 120–130 m lower than today (Lambeck et al., 2014; Peltier, 2002), exposing extensive shelf areas. Deglacial sea-level rise and glacial isostatic adjustment (GIA)—including uplift and subsidence of the ocean floor—have since flooded these

Visualization: S. L. Ward
Writing – original draft: S. L. Ward
Writing – review & editing: S. L. Bradley, S-B. Wilmes, Z. A. Roseby, J. A. M. Green, P. E. Robins, C. M. Roberts, J. D. Scourse

regions, reshaping tidal dynamics on a global scale (e.g., Egbert et al., 2004; Green, 2010; Schmittner et al., 2015; Sulzbach et al., 2023; Wilmes & Green, 2014; Wilmes et al., 2023). However, despite the global importance of continental shelf seas and their tidal dynamics, some regions, such as the Patagonian Shelf, remain underexplored.

Shelf sea hydrodynamics are acutely sensitive to sea-level fluctuations, which can alter tidal resonance (Green, 2010), tidal residuals (e.g., Guo et al., 2018; Neill et al., 2010), tidal propagation, amplification, and phasing (e.g., Carless et al., 2016; Müller et al., 2011; Schindelegger et al., 2018; Ward et al., 2016; Ward et al., 2012), and sediment transport (e.g., Hall & Davies, 2004; Van der Molen & De Swart, 2001; Ward, Bradley, Roseby, et al., 2025). These changes to tidal dynamics can in turn drive alterations in habitat distribution, seasonal stratification (Hayden et al., 2020; Simpson & Hunter, 1974), and biogeochemical functions including primary productivity and CO_2 fluxes (e.g., Chavez et al., 2011; Falkowski et al., 1998; Rippeth et al., 2008).

Understanding seasonal stratification and tidal mixing is important because these are processes which link tidal dynamics to long-term carbon cycling across continental shelf seas. Although contemporary continental shelf seas cover just 7% of the ocean's surface, they are key drivers of ocean-atmosphere CO_2 exchange, linking the terrestrial, atmospheric and oceanic carbon reservoirs (Thomas et al., 2004). The balance between tidal mixing and surface heating controls the formation of tidal mixing fronts, which delineate well-mixed and seasonally stratified waters and strongly influence nutrient supply, primary productivity and uptake of CO_2 from the atmosphere. Following post-glacial sea-level rise, the tenfold expansion of global shelf seas (De Groeve et al., 2022) greatly increased their role in atmosphere-ocean CO_2 exchange by enhancing biological carbon uptake and long-term organic carbon burial (Rippeth et al., 2008). An empirically derived stratification parameter linking water depth and M_2 tidal current speeds allows the position of tidal mixing fronts to be approximated (Bowers & Simpson, 1987; Simpson & Hunter, 1974, Section 2.3.3 below). Tidal model outputs can therefore be used to reconstruct past seasonal stratification patterns, which offer insights into long-term carbon cycling across temperate shelf seas (Rippeth et al., 2008; Woods et al., 2019).

High-resolution modeling of past tidal regimes is essential to our understanding of long-term shelf sea evolution, and offers insights which cannot be inferred from observations. Paleotidal simulations differ from models of contemporary tides by incorporating relative sea-level history through paleotopography derived from GIA modeling. To account for time-varying changes in global tides, paleotidal models also derive boundary conditions from a global paleotidal model. At regional scales, such simulations have wide-ranging applications, from refining sea-level index points to informing archeological and ecological reconstructions (Scourse, 2013; Uehara et al., 2006; Ward, Bradley, Roseby, et al., 2025). Predictions of tidal currents and bed shear stress also enable hindcasting of large-scale sediment dynamics (e.g., Scourse et al., 2009; Van der Molen & De Swart, 2001), providing insights into coastal evolution, habitat change and blue carbon storage potential in seabed sediments (Ward, Bradley, Roseby, et al., 2025). Tidal energy dissipation, arising from friction between tidal currents and the seabed (Taylor, 1920), drives vertical mixing that supports components of large-scale ocean circulation, including the Meridional Overturning Circulation (Ladant et al., 2024; Munk, 1997; Melet et al., 2022; Wilmes et al., 2023), further emphasizing the broader climatic relevance of reconstructing past tidal dynamics.

Although past sea levels are needed as input into palaeotidal models, reconstructing past sea levels themselves requires an understanding of past tides, because variability in the tidal range affects the interpretation of observations of past sea levels. Relative sea-level reconstructions (e.g., Bradley et al., 2011) can be derived using GIA modeling, which incorporates ice-sheet history, mantle viscosity, and crustal response to changing loads. The observational data used as input to a GIA model are typically sea-level index points, which are geological or biological markers of past sea levels. Because GIA models inform boundary conditions for paleotidal simulations, the reconstruction of past sea levels and tidal regimes is inherently iterative, requiring ongoing refinement as new data and methods emerge.

This study presents the first high-resolution paleotidal reconstruction of the Patagonian Shelf from the LGM (taken as 21,000 years before present, "ka BP") to present. Using updated paleotopography and ocean boundary conditions, we simulate tidal dynamics and relative sea-level change for 1 ka time slices, quantifying changes in tidal elevation amplitudes, tidal energy dissipation and seasonal stratification. We also examine point-based estimates of changes in Mean High Water Spring Tide (MHWST) through time. These freely-available tidal simulations (Ward, Bradley, & Wilmes, 2025) provide new insights into the past evolution of this tidally energetic shelf sea and its role in the Earth system.

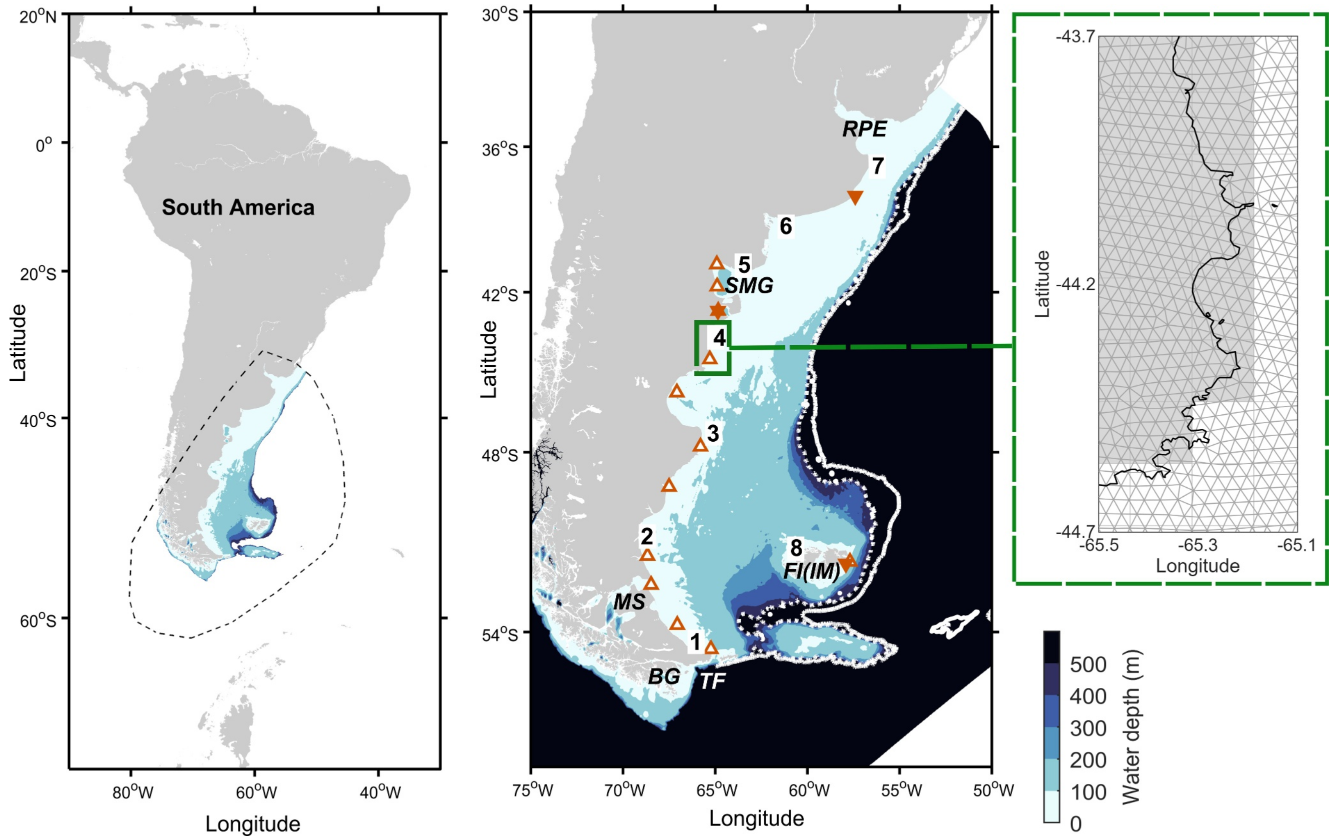

Figure 1. Left: Model domain of the Patagonian Shelf model (dashed black line) within the wider regional context. Water depth is shown using a blue color scale, displaying only depths shallower than 500 m. Middle: Present-day bathymetry of the Patagonian Shelf with 500 m (dotted white line) and 1,000 m (solid white line) depth contours. Orange triangles mark the coastal tide gauges used for model validation (outlined triangles: Moreira et al. (2011); filled triangles: Piccioni et al. (2019)). Numbers 1–8 indicate sites where relative sea-level curves and Mean High Water Spring Tide (MHWST) time series were extracted. Place names referred to in the text are: (FI/IM) Falkland Islands/Islas Malvinas; (RPE) Río de la Plata Estuary; (SMG) San Matías Gulf; (MS) Magellan Straits; (BG) Bahía Grande; and (TF) Tierra del Fuego. Right, green bounding box: Comparison of model grid resolutions. The global ocean model uses a coarser regular grid (gray land cells and white water cells), while the regional tidal model uses a higher-resolution unstructured triangular mesh (gray triangles). The present-day coastline is shown in black.

1.1. Study Area: The Patagonian Shelf

Here we present results for the model domain covering the continental shelf between approximately 35°S and 55°S (Figure 1), which lies off the southeastern coast of South America. This domain encompasses what is variously referred to in the literature as the South Western Atlantic Continental Shelf, the Argentine Continental Shelf, or the Argentine Sea (*Mar Argentino*), among others. The region is referred to here as the Patagonian Shelf, consistent with usage in previous tidal and shelf sea modeling studies (Combes & Matano, 2018; Carless et al., 2016; Glorioso, 2000; Glorioso & Flather, 1997; Glorioso & Simpson, 1994; Luz Clara et al., 2015), as well as the TPXO atlas product for the Patagonian Shelf (Egbert & Erofeeva, 2002). This domain is also consistent with the Patagonian Shelf Large Marine Ecosystem (LME) framework (GEF LME:LEARN, 2017).

The Patagonian Shelf is an oceanographically complex shelf sea that has undergone repeated cycles of exposure and submersion over glacial-interglacial timescales. Extending ~2,400 km southward from ~32°S and oriented northeast to southwest, its width ranges from ~170 to 850 km, averaging ~400 km (Figure 1a; Violante et al., 2014 and references therein). This relatively shallow shelf features four terraces separated by steep, high-gradient steps (Violante et al., 2014). With average depths of ~115 m and typically <150 m, much of the shelf was exposed during past sea-level lowstands (Guilderson et al., 2000; Violante & Parker, 2004). Cycles of exposure and flooding have shaped its sedimentology and bathymetry, with bathymetric terraces linked to interruptions in sea-level rise during past marine transgressions, forming cliff-like erosional features along paleo-shorelines (Violante, 2005).

Oceanographic conditions on the Patagonian Shelf are shaped by a combination of sub-Antarctic water masses, strong winds, and regional tidal currents. Shelf waters originate predominantly from cold, nutrient-rich sub-Antarctic sources, while the mean flow and net export of surface waters are directed northeastwards (Violante et al., 2014). Circulation is influenced by the Malvinas/Falkland Current (Ruiz Etcheverry et al., 2016), freshwater input from the Magellan Straits (Palma et al., 2008) and persistent wind forcing. The Patagonian Shelf is one of the most tidally energetic regions globally, with strong tidal currents and large tidal ranges. The southern shelf is near-resonant for the semidiurnal M_2 constituent (Webb, 1976), with elevation amplitudes (which are half the tidal range) reaching ∼4 m in some areas. The S_2 constituent can reach ∼1 m elevation amplitude in the southern sector (Gil et al., 2019). These amplitudes drive strong tidal currents—M_2 currents exceed 1.5 m/s in parts of the southern shelf (Palma et al., 2004)—which are key to sediment transport and mixing. Vertical mixing by tidal currents forms tidal mixing fronts that separate stratified and well-mixed regions (Simpson & Hunter, 1974). Seasonally stratified mid- and off-shelf areas of the Patagonian Shelf have been identified as important CO_2 sinks, even during summer months, because phytoplankton blooms on the stratified side of tidal fronts reduce surface pCO_2 well below atmospheric levels, sustaining air-sea CO_2 uptake despite stratification (Bianchi et al., 2005). While semidiurnal tides dominate, diurnal constituents (K_1 and O_1) reach up to ∼0.25 m in Bahía Grande, with potential local effects on coastal circulation and biological processes. This study focuses on shelf-scale tidal dynamics; for broader oceanographic context, see Gil et al. (2019) and Violante et al. (2014).

Tidal modeling of the Patagonian Shelf has primarily focused on present-day conditions, with limited exploration of past dynamics. Previous studies have examined contemporary tidal dynamics (Carless et al., 2016; Glorioso, 2000; Glorioso & Flather, 1995, 1997; Glorioso & Simpson, 1994; Luz Clara et al., 2015; Moreira et al., 2011; Simionato et al., 2004), while Carless et al. (2016) and Luz Clara et al. (2015) considered future sea-level rise scenarios. More recent hydrodynamic modeling by Dinápoli et al. (2020, 2024) and Dinápoli and Simionato (2024, 2025) extends beyond tide-only approaches. Alonso et al. (2025) present the first paleotidal model for the San Matías Gulf at 11.5 ka BP. To date, no studies have examined past tidal conditions across the entire Patagonian Shelf since the LGM.

2. Methods

Our paleotidal model development consisted of three main steps. First, we reconstructed regional relative sea-level change using a revised global GIA model (Section 2.1), providing the evolving paleotopography needed for both global and regional simulations. Second, we used this paleotopography as input to a global paleotidal model (Section 2.2) to obtain time varying tidal boundary conditions. Third, these boundary conditions were applied to a new high resolution palaeotidal model of the Patagonian Shelf (Section 2.3), which we used to simulate regional tidal dynamics over the past 21,000 years.

2.1. Generation of Relative Sea-Level Predictions

The tidal models (both global and regional) and the global GIA model require an ice sheet reconstruction as an input, which defines the spatial and temporal extent of the large, continental-scale grounded ice sheets. For this study, we used the PaleoMIST1.0 data set (Gowan et al., 2021), a global ice sheet reconstruction for the past 80 ka, which was developed independently of sea level observations or $\delta^{18}O$ data, reducing the inherent circularity mentioned above. Chronological, geological and geomorphological constraints were used to constrain the ice-sheet margins within the PaleoMIST1.0 framework, combined with a plastic ice sheet model (Gowan et al., 2016). The Patagonian ice sheet component of PaleoMIST1.0 was constrained using the reconstruction of Darvill et al. (2016).

Within the GIA modeling framework, tectonic setting exerts a strong control on Earth rheology. As the western margin of Chile is tectonically active due to the subduction of the Nazca Plate, we adopted a weaker upper mantle viscosity in the Earth component of the GIA model than is typically used in more passive margin settings, as supported by studies investigating relative sea level and crustal uplift along this margin (Garrett et al., 2020; Lange et al., 2014). We used a 1D, spherically symmetrical Maxwell viscoelastic Earth model with a lithosphere thickness of 96 km and an upper and lower mantle viscosity of 5×10^{19} Pas and 1×10^{22} Pas, respectively. The GIA model solves the generalized sea level equation (Kendall et al., 2005; Mitrovica & Milne, 2003) and includes time-dependent shoreline migration, perturbations to the Earth's rotation vector, and sea-level changes in regions of retreating marine-based ice. The resulting relative sea-level reconstructions do not incorporate steric (density-driven) changes, as postglacial sea-level rise is dominated by barystatic contributions from melting ice sheets (Gebbie, 2020).

The GIA model was solved to a maximum spherical degree of 512, corresponding to a grid size of approximately 0.35° in latitude and longitude. All ice-sheet thickness and relative sea level data sets can be found at Ward, Bradley, and Wilmes (2025).

2.2. Ocean Model Forcing: Global Paleotidal Model

Global tidal boundary conditions for the regional model were generated using the Oregon State University Tidal Inversion Software (OTIS) in its forward mode (e.g., Egbert & Erofeeva, 2002; Egbert et al., 2004; Green & Nycander, 2013; Wilmes et al., 2023). OTIS solves the linearized shallow water equations (e.g., Hendershott, 1972) without horizontal advection, and incorporating energy dissipation through bed friction and tidal conversion:

$$\frac{\partial U}{\partial t} + f \times U = -gh\nabla(\eta - \eta_{\mathrm{SAL}} - \eta_{EQ}) - F \quad (1)$$

$$\frac{\partial \eta}{\partial t} + \nabla \cdot U = 0 \quad (2)$$

Here, $\mathbf{U} = h\mathbf{u}$ is the depth-integrated tidal volume transport ($\mathbf{u}$ is the horizontal velocity vector and h is the water depth), $\mathbf{f}$ is the Coriolis parameter, g is acceleration due to gravity, η is the sea-surface elevation, η_{SAL} is the self-attraction and loading elevation, η_{EQ} is the elevation of the equilibrium tide, and $\mathbf{F}$ the tidal energy dissipation term. The latter is a sum of two components, $\mathbf{F}_{\mathrm{B}}$ and $\mathbf{F}_{\mathrm{W}}$, where $\mathbf{F}_{\mathrm{B}}$ parameterizes bed friction and $\mathbf{F}_{\mathrm{W}}$ represents energy losses due to tidal conversion, that is, the transfer of energy into a baroclinic tide. The first term is represented using the standard quadratic law, $\mathrm{F_B} = C_{\mathrm{D}}\, \mathbf{u}|\mathbf{u}|$, where $C_{\mathrm{D}} = 0.003$ is a dimensionless drag coefficient. The tidal conversion term is given by $\mathrm{F_W} = C\mathbf{U}$, with a conversion coefficient, C, given by Green and Nycander (2013) and Zaron and Egbert (2006):

$$C(x,y) = \gamma \frac{N_H \underline{N}}{8\pi\omega}(\nabla H)^2 \quad (3)$$

Here, $\gamma = 50$ represents a dimensionless scaling factor representing unresolved bathymetric roughness, N_H is the buoyancy frequency at the seabed, $\underline{N}$ represents the vertical average of the buoyancy frequency, and ω is the frequency of the tidal constituent under consideration. The buoyancy frequency, N, is given by $N^2 = -g/\rho\, \partial\rho/\partial z$, where ρ is the density.

The configuration used here follows that of Wilmes et al. (2023), also used in Ward, Bradley, Roseby, et al. (2025). Global simulations were performed at a 1/8° × 1/8° horizontal resolution and included the tidal constituents M_2, S_2, K_1 and O_1, these being the dominant semi-diurnal and diurnal tides globally. The global model domain extends from 86°S to 89°N where it is bounded by an artificial vertical wall which eliminates the need for open boundary conditions. Present-day bathymetries were based on RTOPO-2 (Schaffer et al., 2016), which integrates GEBCO_2014 data (Weatherall et al., 2015). Paleobathymetry preparation followed the approach described in Wilmes et al. (2023), incorporating the latest glacial isostatic model for the region (see previous section). These relative sea-level changes were interpolated to the global model grid and added to the RTOPO-2 baseline topography, to define the water depth (h) for each 1 ka time interval. Ice sheets extending over the ocean were assumed to be floating. Simulations were conducted at 1 ka intervals, from 21 ka to 0 ka BP. Equilibrium tidal constituents were held fixed at modern values for all simulations, as changes to the equilibrium tidal component over this time are negligible in comparison to dynamic changes resulting from variations in water depths and coastline configurations. For detailed validation of the present-day control run and for further details on model parameterization, refer to Wilmes et al. (2023).

2.3. Regional Tidal Model

A new regional paleotidal model for the shelf was developed because the global model, at 1/8° resolution (∼10–15 km), cannot resolve the complex coastline and bathymetric gradients of the Patagonian Shelf (Figure 1),

10.1029/2025PA005384

which strongly influence tidal propagation and dissipation. Computational considerations also justify the regional approach: here the regional model was >70 times cheaper computationally per 1 ka time interval.

2.3.1. Hydrodynamic Model Set-Up

We applied TELEMAC-2D (version 8p5r0), an open-source hydrodynamic modeling system (www.opentelemac.org) which solves the 2D Saint-Venant equations (Equations 4 and 5 for continuity and momentum, respectively), that is, the non-linear shallow water equations (Hervouet, 2000):

$$\frac{\partial h}{\partial t} + \nabla \cdot (hu) = S_h \quad (4)$$

$$\frac{\partial (hu)}{\partial t} + \nabla \cdot (h\, u \otimes u) = -g\, h \nabla \eta + \nabla \cdot (h\mathbb{D}) + h\mathrm{F} + S_{xy} \quad (5)$$

where h is the water depth, $\boldsymbol{u} = (u,v)$ the depth-averaged velocity components, S_h a mass source term, η the free surface elevation, g the gravitational acceleration, $\mathbb{D}$ the dispersion-diffusion tensor, $\boldsymbol{F} = (F_u, F_v)$ is the combined momentum-source vector, S_{xy} represents the momentum source terms (including the Coriolis force, bottom friction etc.), and $u \otimes u$ denotes the outer (tensor) product, whose divergence gives the non-linear momentum-advection terms. As is the case for the ocean model (Section 2.2), the water depth used in these equations is derived from the relative sea level.

The hydrodynamic model was run in finite element mode, based on an unstructured triangular computational mesh grid (Figure 1), facilitating increased model resolution on the continental shelf and in coastal areas, with coarser resolution extending off-shelf, to up to 18–20 km. The unstructured grid capability optimizes the resolution of coastal processes and computational efficiency. The mesh edge lengths were set to 2 km at the narrow shelf edge and restricted to between 2 and 4 km on the shelf. The entire model domain, including some grid cells over land, was gridded, and the model incorporated alternate wetting and drying of coastal nodes flooded by the tide. This approach maintains all finite elements in computation, while allowing dry land and ensures mass conservation. This method was chosen for its ability to maintain a consistent computational grid across model runs, accommodating evolving coastlines and intertidal cells in response to changing relative sea level driven by GIA and ice sheet extent.

The GEBCO_2023 digital terrain model (GEBCO Compilation Group, 2023) was used, providing a global representation of both land and ocean topography (15-arc seconds grid resolution). For the present-day model, GEBCO_2023 data were interpolated onto the model's unstructured mesh. This grid also served as the foundational bathymetric data set for the paleotidal simulations. At each 1 ka paleo-time slice, the relative sea level (Section 2.1) was applied to the GEBCO_2023 bathymetry. Consequently, the water depth used by the model for each 1 ka time interval was derived from the relative sea level data set for that time slice. Finally, the grounded ice sheet extent for each time slice was incorporated into the paleotopography, using the same ice sheet reconstructions as those implemented in the GIA model (Section 2.1).

The data on ice sheet thickness and extent used in this TELEMAC model represent only grounded ice, with no parameterization for floating ice. In studies reconstructing past sea levels, the volume of grounded ice is typically used, and may be referred to as the "ice-volume equivalent sea level" (see Bradley et al. (2016) for further details). More recently, this concept has also been described as "barystatic sea level" or "global-mean sea level" (Gregory et al., 2019). For ease of data analysis and for subsequent use of output by others, model output was interpolated onto a structured 1/50° grid extending from approximately 52°–71°W and 35°–55.5°S, and within 1,000 m depth contour on the shelf edge. This spatial constraint was applied because the primary focus of this study is on tidal dynamics and sea-level processes over the Patagonian Shelf, and model validation was conducted using observational data from the shelf region (Section 2.3.2).

The model is barotropic and does not include any tidal conversion parameterization. Carless et al. (2016) suggested that tidal dissipation due to the internal tide (i.e., tidal conversion) on the Patagonian Shelf was almost an order of magnitude lower than tidal dissipation due to bottom friction. The tidal propagation on the shelf was reasonable without this parameterization (see present-day validation) and because the uncertainties in the paleotidal forcings are likely to be greater than the effects of this parameterization, our use of a barotropic tidal model

Table 1
Validation Results for the Present-Day Regional Depth-Averaged Barotropic Tidal Model, Using Coastal Tide Gauge Data From Piccioni et al. (2019; "TICON") and Moreira et al. (2011; "MOREIRA")

	M_2				S_2			
	Amplitude		Phase		Amplitude		Phase	
	RMSE (cm)	SI (%)	RMSE (°)	SI (%)	RMSE (cm)	SI (%)	RMSE (°)	SI (%)
TICON (n = 3)	8	9	6	2	6	2	5	4
MOREIRA (n = 12)	27	11	13	7	–	–	–	–

Note. RMSE = root mean square error; SI = scatter index (RMSE normalized by the mean of the data).

is assumed justified. For parameterization of bottom friction, a constant friction coefficient of 0.25 was used in Nikuradse's law of bottom friction (Hervouet, 2000). The turbulence model with a constant viscosity coefficient was used, which represents the molecular viscosity, turbulent viscosity, and dispersion. The velocity diffusivity within this turbulence model was $1e^{-6}$ m^2/s, corresponding to the molecular viscosity of water. Each model was run for a 25-day period, the latter 20 days of which were output for analysis (including harmonic analysis used in the model validation), which excluded five days of model spin-up, sufficient for tides-only simulations of this domain. This is in accordance with the Rayleigh criterion, which states that two constituents are resolvable when their frequency difference exceeds the inverse of the record length. Using the astronomical frequencies of the constituents applied here, the closest pair is M_2-S_2, which requires ∼14.8 days to resolve. K_1 and O_1 have a larger separation and require ∼10 days. Our 20-day simulation exceeds both requirements and is therefore sufficient for resolving M_2, S_2, K_1 and O_1. Simulated water depth, surface elevation and u- and v-components of current velocity were output at model grid nodes at 30-min (instantaneous) intervals. The present-day regional model was forced at its offshore boundaries using harmonic constants derived from the global ocean tidal model (Section 2.2). The boundary forcing comprised surface elevation and depth-averaged tidal current velocities for the M_2, S_2, K_1, and O_1 tidal constituents. These global model outputs used as regional paleotidal forcings were available at 1 ka time intervals, from 21 ka BP to present day.

2.3.2. Regional Model Validation

The elevation amplitudes of the M_2 and S_2 tidal constituents were extracted from the model output via harmonic analysis (T_TIDE, Pawlowicz et al., 2002) and compared with observed harmonic constants (Table 1). Tide gauge data from a combination of published sources were used, comprising three coastal tide gauges in the TICON data set (Piccioni et al., 2019; Figure 1) and 12 tide gauges from Moreira et al. (2011; Figure 1), although variation existed in which tidal constituent harmonics were available between the sources. There are very limited observational tide gauge data from the Patagonian Shelf, particularly for measurements taken in offshore waters (e.g. deeper than 10 m).

2.3.3. Calculating Tidally Modulated Parameters

2.3.3.1. Seasonal Stratification

We use the dimensionless stratification parameter ($\chi \propto h/u^3$), with a critical contour at $\log_{10}(\chi) = 2.5$ (Bowers & Simpson, 1987) to estimate the position of tidal mixing fronts, where, h is the water depth and u is the depth-averaged M_2 tidal current speed. This provides a shelf-wide approximation for seasonal stratification: regions where $\log_{10}(\chi) \leq 2.5$ are expected to remain well mixed throughout the year, whereas vertically stratified waters occur where $\log_{10}(\chi) > 2.5$.

2.3.3.2. Tidal Energy Dissipation

Here we assess energy dissipation associated with individual tidal constituents, as resolved using the T_TIDE harmonic analysis package (Section 2.3.3). We consider a parameterization for (barotropic) tidal energy dissipation resulting from friction with the seabed, such that:

$$D_{\mathrm{fric}} = \rho C_D |\boldsymbol{u}|^3 \tag{6}$$

where C_d is a dimensionless bottom drag coefficient (∼0.003) and $\boldsymbol{u}$ is tidal velocity vector, taken as a mean over a tidal cycle (Taylor, 1920). The value of u can be obtained by scaling the constituent-specific velocity amplitudes by 0.636, to represent the mean absolute value of a sine wave with amplitude of 1 (i.e., u represents the cycle-mean absolute velocity, which is then cubed in this formulation). Again, note that this parameterization ignores tidal energy lost to conversion (i.e., to the internal tide at the shelf edge) as this was not simulated by this model, and which has previously been shown to be of an order of magnitude lower than energy losses due to friction (Carless et al., 2016). To approximate shelf-wide tidal dissipation, we include only water depths <200 m (following the methods of Carless et al., 2016). Values from very shallow areas (<5 m) are excluded due to grid interpolation between land and sea, which can produce unreliable estimates near the coast. As water depths varied over time, this depth criterion was applied at each time slice using the corresponding water depth for that time.

3. Results

3.1. Evolution of the Patagonian Shelf Since the LGM

At 21 ka BP, during the LGM, the areal extent of the Patagonian Shelf sea (defined here as regions with water depth <200 m) was substantially reduced due to lower eustatic sea levels and GIA associated with extensive ice sheet coverage (Figure 2). At this time, the shelf sea covered only 29% of its present-day extent. This limited area persisted until around 18 ka BP, with only gradual expansion (to ∼36%) during the early deglacial phase. The most rapid increase in shelf sea area occurred between 18 and 14 ka BP, driven by accelerated sea-level rise, expanding from ∼36% to ∼80% of its modern extent. By 12 ka BP, the shelf sea had reached approximately 90% of its current size, and the modern coastline configuration was largely established (>99%) by 8 ka BP.

At present, the Islas Malvinas/Falkland Islands are separated from mainland South America by waters exceeding 150 m deep (at mean sea level). New relative sea-level reconstructions presented here suggest that this separation persisted throughout the study period, with no indication of a land bridge during the LGM. However, the intervening waters were significantly shallower in the past, with mean depths of ∼25–50 m between 21 and 18 ka BP.

3.2. Changing Tidal Dynamics Across the Shelf

Tidal dynamics on the Patagonian Shelf have evolved significantly since the LGM, shaped by changes in sea level, shelf geometry, and resonance effects. The semi-diurnal M_2 (principal lunar) constituent dominated tidal dynamics since the LGM, with maximum elevation amplitudes an order of magnitude larger than any other constituent around 10–9 ka BP. In general, M_2 elevation amplitudes have increased with inundation of the shelf since 21 ka BP (Figure 3 and Figure S2 in Supporting Information S1), with present-day amplitudes largely having been established by 1 ka BP and remaining higher than at any earlier time period considered here. Consistently, the highest M_2 elevation amplitudes have been across the southern part of the shelf, exceeding 4 m in the present day off Tierra Del Fuego. Similarly, present-day S_2 (principal solar) tidal elevation amplitudes, reaching up to ∼1.3 m, are the highest across the simulated period and were considerably lower prior to 1 ka BP, with S_2 clearly the second-largest constituent in absolute magnitude since 2 ka BP. At each time slice, the largest S_2 amplitudes are found in the mid- and southern sections of the shelf. Earlier in the record, from 21 ka BP to 2 ka BP, S_2 amplitudes remained consistently below 0.75 m, indicating a gradual increase over time as the shelf was flooded. Increasing M_2 and S_2 amplitudes over time suggest enhanced tidal mixing potential, particularly in the southern and mid-shelf regions. These changes likely influenced the development and location of tidal mixing fronts, with implications for seasonal stratification (Section 3.4).

The diurnal tidal components show a contrasting temporal pattern to the semidiurnal constituents. For both K_1 (diurnal luni-solar) and O_1 (diurnal principal lunar) constituents, elevation amplitudes were consistently higher in the past than at present, with values generally greater across the southern shelf than the northern shelf. Peak elevation amplitudes were ∼0.4 m until 15 ka BP (K_1) and ∼0.5 m until 12 ka BP (O_1) followed by gradual decreases in both to present-day (∼0.3 m for each). However, when integrated across the shelf, O_1 constituent was the second largest contribution to the total tidal signal from 21 ka BP to 1 ka BP (S_2 was the smallest), reflecting the broader spatial footprint of the diurnal signals compared with the more spatially localized semi-diurnal (S_2) peaks.

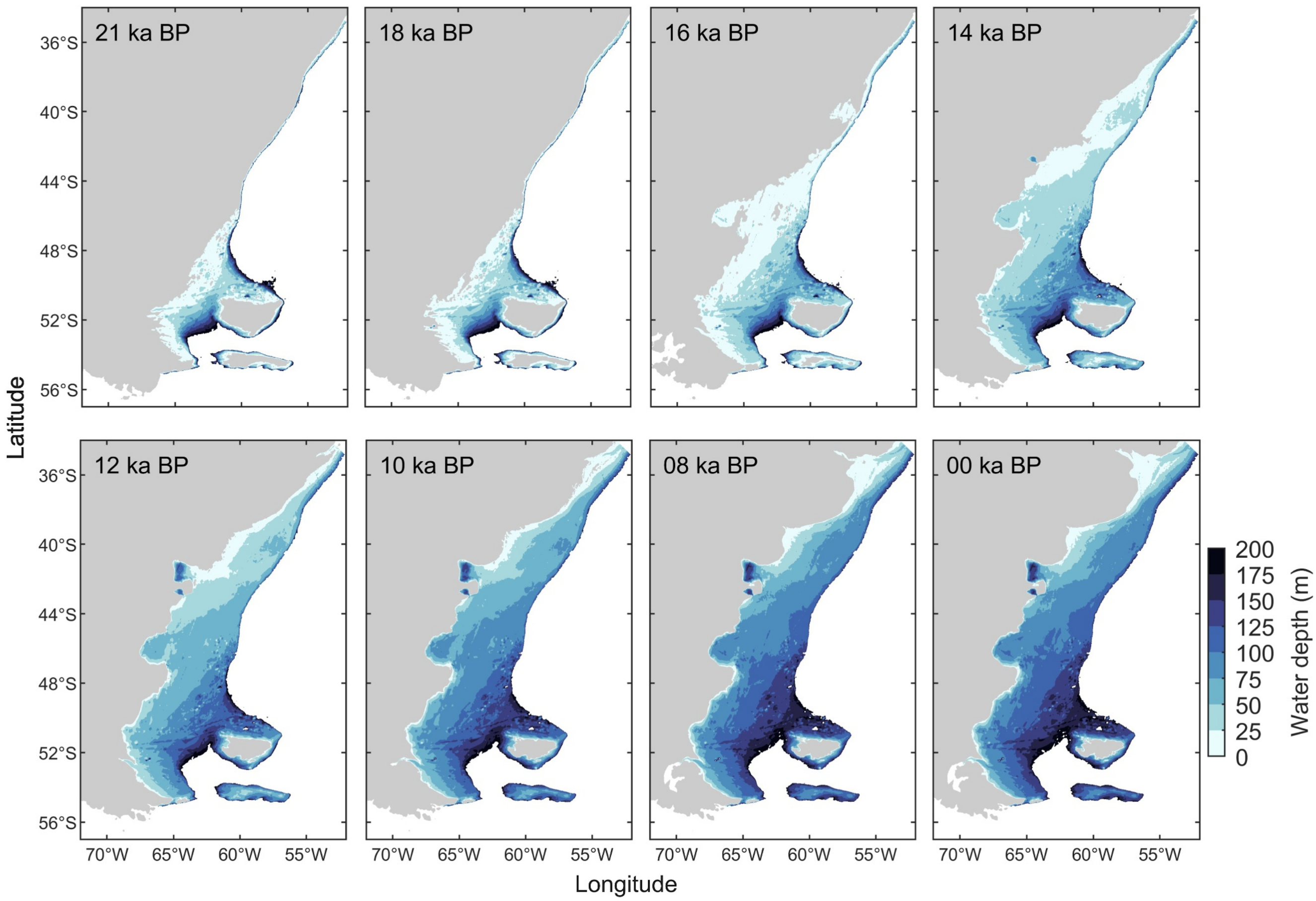

Figure 2. Reconstructed regional bathymetries showing water depth for selected time slices from 21 ka BP (top left) to the present (00 ka BP, bottom right). Only waters shallower than 200 m are plotted to highlight the evolving extent of the continental shelf. Gray areas indicate regions not covered by water, representing either land or grounded ice. A complete set of regional bathymetry and seasonal stratification maps at 1 ka intervals is provided in Figure S1 of Supporting Information S1, and the supporting data are available at Ward, Bradley, and Wilmes (2025).

3.3. Tidal Energy Dissipation

Present day tidal energy dissipation across the Patagonian Shelf is dominated by the M_2 constituent (Figure 4). The total horizontally integrated dissipation rate for M_2 is approximately 148 GW, whereas S_2 and K_1 each contribute less than 2 GW, and O_1 contributes ~2 GW. These values are calculated for regions of the shelf with water depths between 5 and 200 m, within the domain bounded by the 1,000 m contour shown in Figure 1. Dissipation values for all four constituents across each 1 ka time slice are provided in the Supporting Information S1. The following analysis focuses on temporal variability of M_2 relative to present-day.

M_2 tidal energy dissipation has varied substantially over the last 21 ka, reflecting changes in shelf extent and geometry, although its evolution was non-linear and not proportional to shelf area. At 21 ka BP, when the shelf area was greatly reduced (Section 3.1), M_2 dissipation was approximately 50% of the present-day value. Between 21 ka BP and 15 ka BP, dissipation remained relatively high across the southern shelf, but declined considerably by 14 ka BP. By 10 ka BP, the spatial pattern of elevated dissipation was largely established. However, shelf-wide dissipation continued to fluctuate throughout the Holocene, with notable peaks at 10 ka BP and 1 ka BP, when values exceeded present-day levels by 16% and 10%, respectively. The lowest shelf-scale M_2 dissipation occurred at 6 ka BP, at around 35% of the present-day value.

Dissipation of O_1 tidal energy shows a distinct temporal pattern, differing from the other tidal constituents. During the deglacial interval after 17 ka BP, with a peak around 15 ka BP, O_1 dissipation across the shelf consistently exceeded present-day levels, reaching nearly 50% higher at 15 ka BP (~3.5 GW).

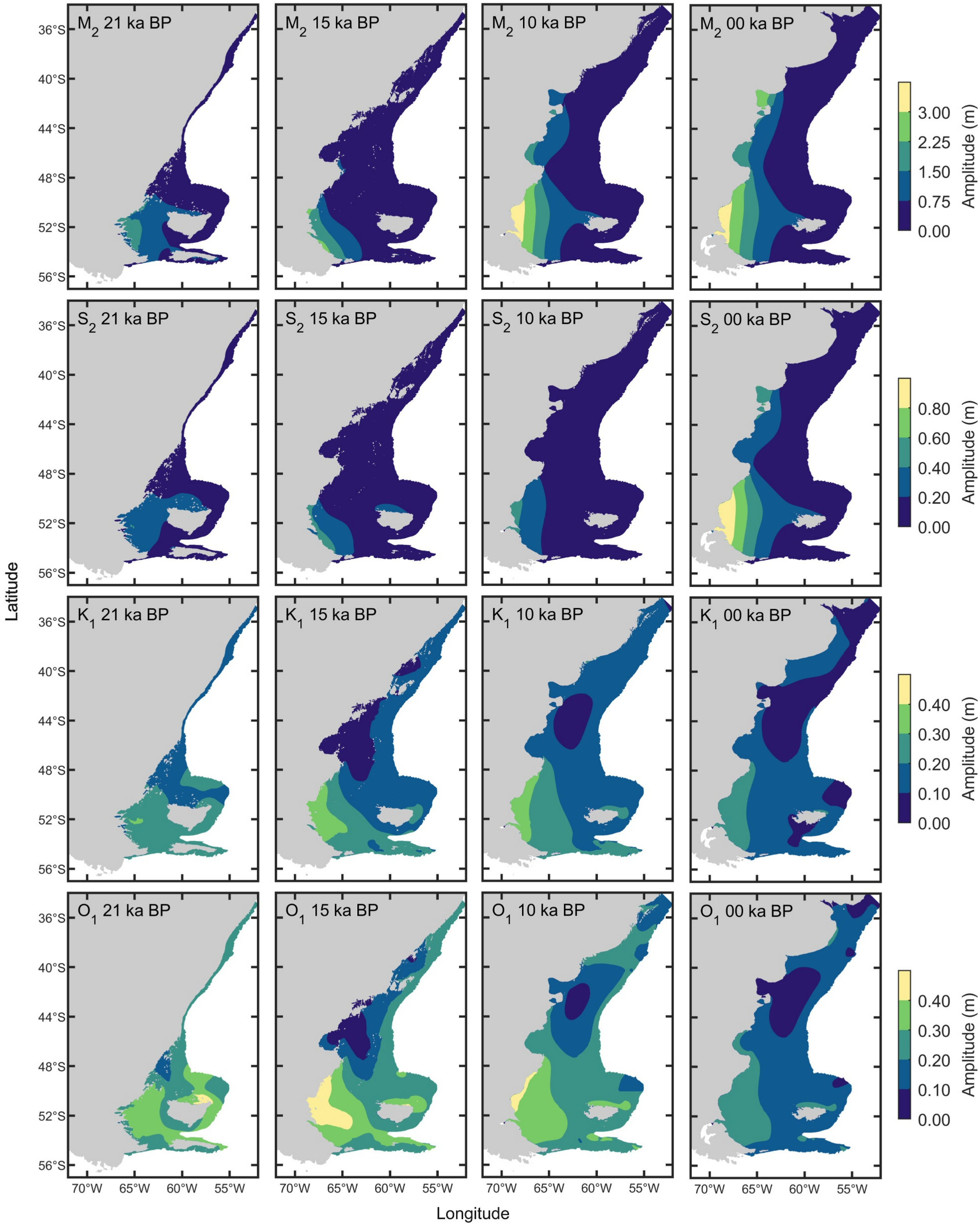

Figure 3. Simulated tidal elevation amplitudes for the four tidal constituents considered here (rows, M_2, S_2, K_1, O_1), shown for selected time slices from 21 ka BP to the present (00 ka BP, columns), for the shelf region within the 1,000 m depth contour. A complete set of regional tidal amplitude maps for all four constituents at 1 ka intervals is provided in Figures S2–S7 of Supporting Information S1. Note the varying colourscales between the constituents.

10.1029/2025PA005384

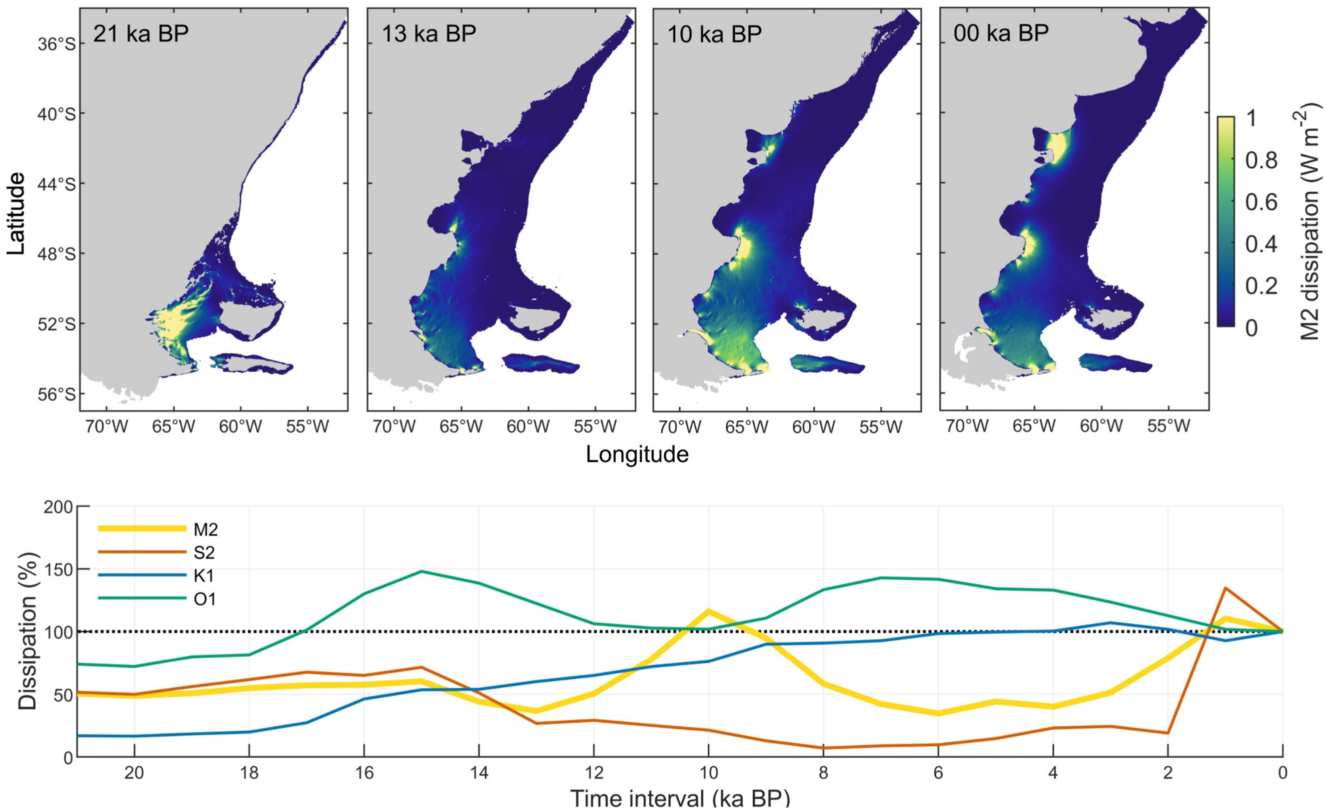

Figure 4. Top panels: Reconstructed maps of M_2 tidal energy dissipation for selected time intervals from 21 ka BP (left) to the present (00 ka BP, right). Color shading indicates the magnitude of dissipation, with only waters shallower than 200 m plotted and gray areas indicate regions not covered by water, representing either land or grounded ice. The present day total M_2 tidal energy dissipation for the domain is 148 GW, whereas dissipation associated with the three other tidal constituents is <3 GW each. Lower panel: Line plot showing the temporal evolution of tidal energy dissipation for the four tidal constituents considered in this study, expressed as a percentage relative to present-day values. A complete set of dissipation maps at 1 ka intervals is provided in Figure S8 of Supporting Information S1, and the data are available at Ward, Bradley, and Wilmes (2025).

The variability in tidal energy dissipation suggests that tidal forcing on the Patagonian Shelf has not simply scaled with shelf area, but has been modulated by evolving resonance conditions and bathymetric complexity. Tidal energy dissipation directly influences vertical mixing, which in turn governs the onset and strength of seasonal stratification—key processes in determining shelf sea functioning.

3.4. Seasonal Stratification

According to the approximation for seasonal stratification ($\chi \propto h/u^3$, Section 2.3.3), 94% of the present-day Patagonian Shelf sea (again, defined here as <200 m depth) is subject to seasonal stratification, with only 6% remaining vertically well-mixed throughout the year (Figure 5, top right panel). In contrast, between 21 and 18 ka BP, less than 75% of the shelf was seasonally stratified (Figure 5), meaning over a quarter remained well-mixed. However, this higher proportion of vertical mixing occurred during a time when the overall shelf sea area was substantially reduced, at only 29%–36% of its modern extent (Section 3.1). As a result, the actual areal extent of seasonally stratified waters at 21 ka BP was only just over 20% of the present-day stratified shelf sea area (Figure 5, dashed line, lower panel).

As the shelf expanded during deglaciation, the proportion of seasonally stratified area increased. Since 10 ka BP, over 90% of the shelf has been seasonally stratified, peaking at 97% around 6 ka BP. Notably, in terms of absolute areal extent, more of the shelf sea was seasonally stratified between 8 and 2 ka BP than today. These shifts in both the proportion and total area of stratified shelf waters likely influenced air-sea carbon fluxes, with implications for long-term carbon cycling across the shelf.

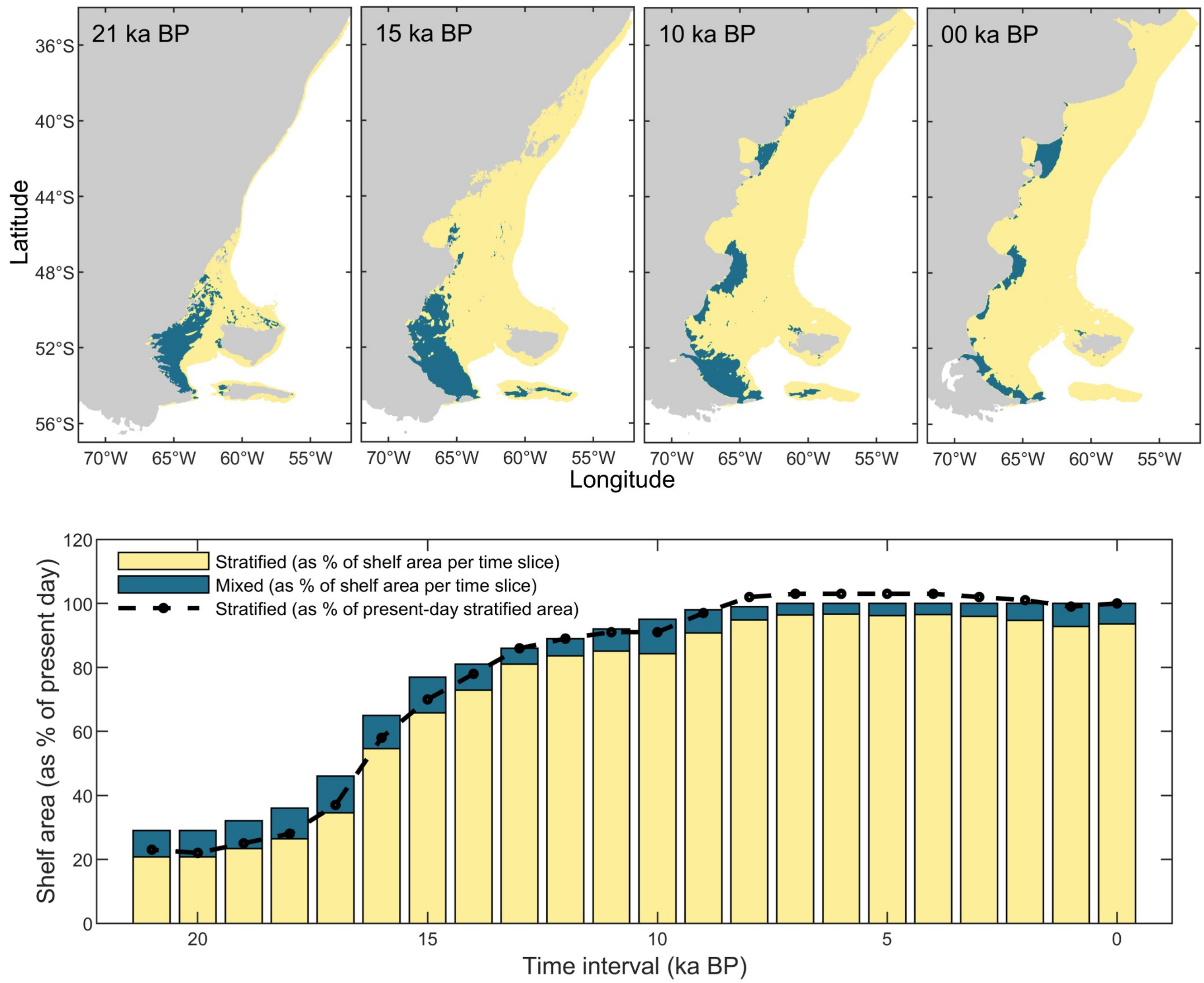

Figure 5. Top panels: Seasonal stratification maps for selected time slices from 21 ka BP to present (left to right). Dark green indicates persistently mixed areas; yellow shows seasonally stratified regions. Lower panel: Stacked bars represent the proportion of mixed and stratified shelf waters at each interval, scaled to the present-day shelf area. The dashed black line shows the extent of stratified waters relative to today. Full 1 ka interval maps are in Figure S9 of Supporting Information S1; data are available at Ward, Bradley, and Wilmes (2025).

3.5. Point-Based Reconstructions of Relative Sea-Level Change and Tidal Evolution

Variability in tidal range is important because many sea-level index points are referenced against MHWST. As MHWST varies through time with changing tidal dynamics, ignoring this variability can introduce significant uncertainty (Hill, 2016). Paleotidal modeling therefore provides essential calibration of vertical datums such as MHWST amplitudes (Leorri et al., 2011; Neill et al., 2010; Ward et al., 2016). Figure 6 illustrates the variation in MHWST relative to present-day values, with temporal changes shown for several example points along the present-day coastline (Figure 1). At each point, the corresponding relative sea-level curve is also provided, indicating that these coastal sites became marine between 12 and 7 ka BP. While the relative sea-level curves are broadly similar across the sites, there is considerable variation in the temporal evolution of MHWST. For example, between 7 and 4 ka BP, MHWST at two southern shelf locations (points 1 and 2) was almost 50% lower than present-day levels. In contrast, during the same period, MHWST at the more northerly point 6 was approximately double (~1 m) the present-day value (~0.5 m). Despite minimal relative sea-level changes at point 7 following inundation at 7 ka BP, the MHWST range increased by over 60% during this time, from 0.15 m to over 0.4 m.

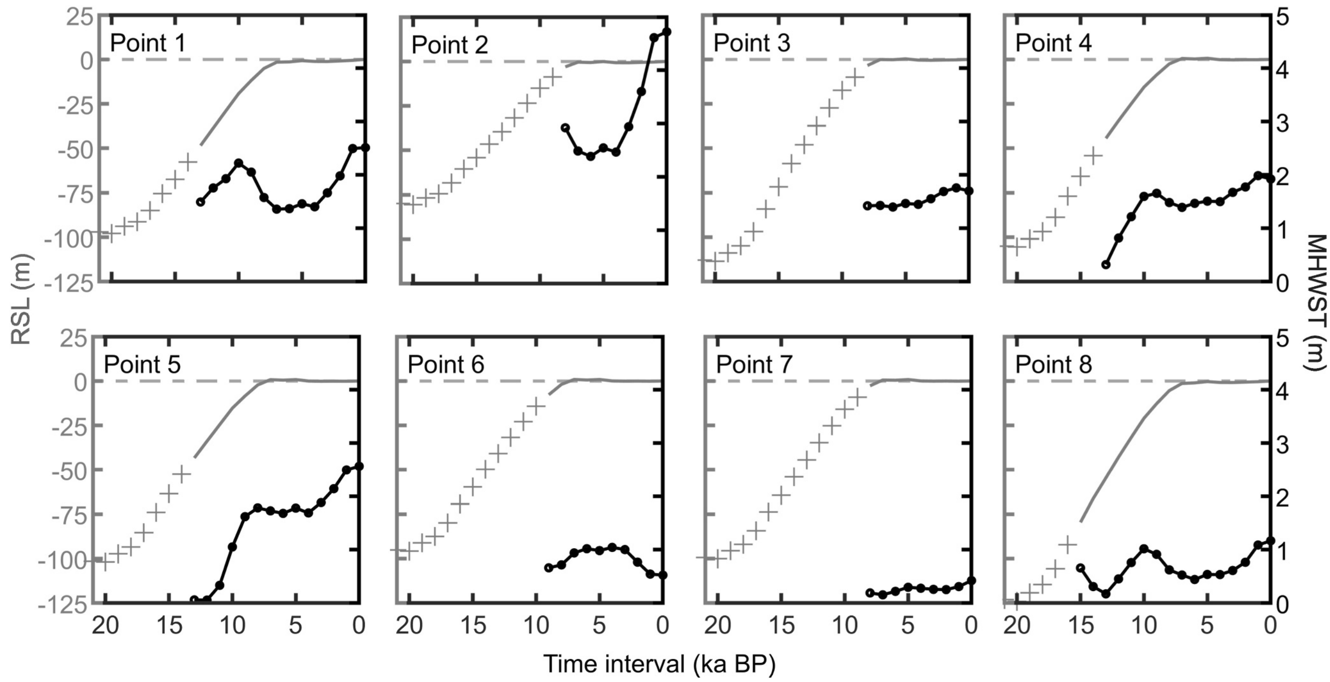

Figure 6. Time series of tidal elevation and relative sea level. Mean high water spring tide (MHWST; black line, right-hand axis) and relative sea level (RSL; gray line and markers, left-hand axis) at the eight point locations shown in Figure 1. MHWST represents the combined $M_2 + S_2$ tidal elevation amplitude. RSL is plotted relative to present-day sea level (0 m at 00 ka BP, gray dashed line). At times when locations were non-marine, MHWST is not shown, and RSL is represented by gray cross markers.

4. Discussion

4.1. Relative Sea-Level History of the Patagonian Shelf

Our results reveal a spatially and temporally complex evolution of tidal dynamics across the Patagonian Shelf since the LGM, driven primarily by relative sea-level change and its influence on shelf extent and coastline morphology. Reconstructing Holocene relative sea-level change in Patagonia remains particularly challenging due to complex vertical land movements and inconsistent interpretations of coastal landforms formed under past sea levels (Pappalardo et al., 2019). The region is under-represented in global sea-level research, with few high-quality relative sea-level curves available (e.g., Bini et al., 2017, 2018; Guilderson et al., 2000; Schellmann & Radtke, 2010), and earlier studies often lacked standardised methodologies and high-resolution elevation data, contributing to uncertainty in defining reliable sea-level index points. Bini et al. (2017) highlight significant spatial variability in Holocene relative sea level across Atlantic Patagonia, emphasizing the need for more precise point-based reconstructions. Our paleotidal model simulations can improve relative sea-level reconstructions by providing time-varying tidal elevations, such as MHWST. These data improve the indicative meaning of sea-level indicators and support calibration or reassessment of existing sea-level index points.

While multiple field-based studies suggest a mid-Holocene highstand of ~2–4 m above present levels along the Atlantic Patagonian coast (e.g., Angulo et al., 2006; Bini et al., 2017; Pappalardo et al., 2019), our GIA simulations do not reproduce such elevated sea levels (Figure 7). For example, Gyllencreutz et al. (2010) report a maximum highstand of +3 m in the Río de la Plata Estuary at ca. 7–5 ka BP, whereas our GIA model yields a substantially lower highstand of only +1 m for the same period. Such discrepancies indicate potential limitations in either model assumptions—such as uncertainties in Earth rheology and ice history—or proxy interpretations.

Milne et al. (2005) showed that the Holocene relative sea level across Southern Patagonia (or South Chile and Argentina) is sensitive to the deglaciation of the west Antarctic ice sheet, delaying the timing of the Holocene highstand by ~2 ka. More recent evidence suggests that the West Antarctic Ice Sheet retreated to a smaller-than-present extent during the Holocene (Lowry et al., 2024), a feature which is not included in PaleoMIST1.0. Addressing these challenges requires integrated approaches combining refined GIA modeling, precise elevation

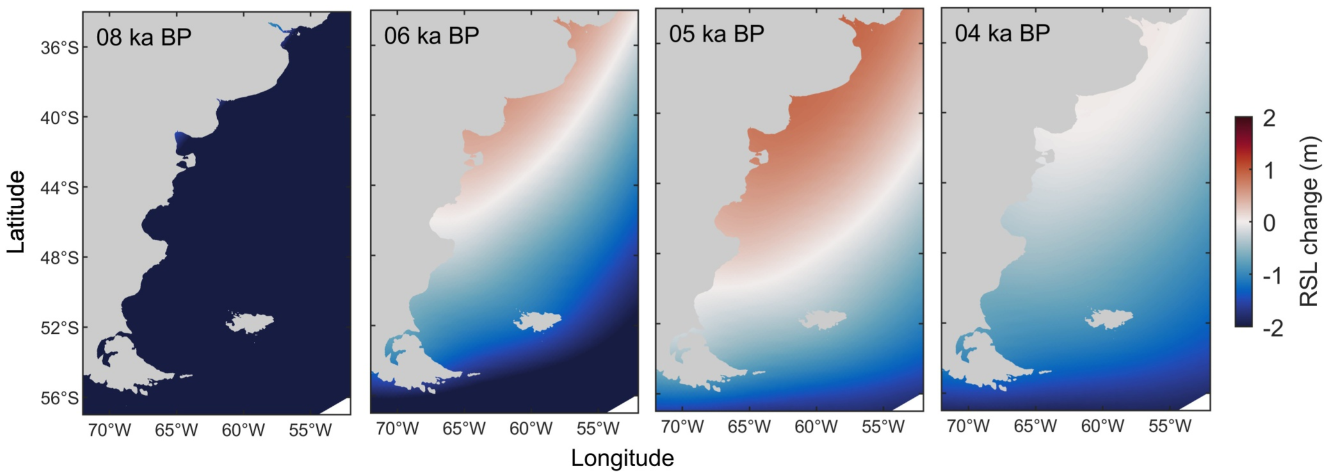

Figure 7. Relative sea-level change. Regional relative sea-level (RSL) estimates for selected time slices, shown as the difference from present-day sea level. Red shading indicates the modest Holocene highstand simulated by the glacial isostatic adjustment model. Note that the present-day coastline and land extent are shown in gray.

data, and re-evaluation of sea-level indicators alongside corrections for paleotidal amplitudes, as demonstrated here (Section 3.5).

4.2. Paleogeographic and Biogeographic Connectivity

The paleogeographic relationship between the Islas Malvinas/Falkland Islands and the South American mainland remains a topic of ecological and biogeographical interest, particularly in the context of past land-sea configurations. High-resolution reconstructions enabled by our GIA model refine understanding of sea-level change and shelf exposure, and hence potential connectivity during key periods such as the LGM.

For example, the extinct Falkland Islands wolf (*Dusicyon australis*, or "warrah"; Hamley et al., 2021), the only native terrestrial mammal on the islands, is thought to have become isolated from its mainland ancestor around 16 ka BP (31–8 ka BP; Austin et al., 2013). Austin et al. (2013) speculated that sea-level lowstands of −130 to −150 m may have narrowed the strait between the islands and mainland South America to 20–30 km, with water depths of 10–30 m. This was potentially shallow and cold enough to freeze seasonally, forming a transient ice-covered bridge or enabling ice rafting. These estimates were based on Ponce et al. (2011), who reported a LGM lowstand of 120–140 m at ∼24 ka BP. However, more recent work has questioned the feasibility of a continuous sea-ice bridge (Hamley et al., 2021), and our relative sea-level estimates support this. Although our model does not include a 24 ka BP time slice, adjacent time slices indicate relative sea levels of −115 m at 25 ka BP and −125 m at 22.5 ka BP. Paleobathymetric reconstructions suggest that even at 21 ka BP, the islands were separated from the mainland by waters over 30 m deep, with relative sea level ∼130 m lower than present. At 21 ka BP, the nearest land points (mean sea level >0 m) were over 150 km away, due west of the islands, and by 16 ka BP, the closest mainland was over 300 km to the southwest, near Tierra del Fuego. Hamley et al. (2021) speculate that, rather than arriving via natural migration, the warrah may have been introduced by early seafaring peoples. This particular discussion highlights the value of our model outputs in constraining paleogeographic scenarios and refining interpretations of biogeographic connectivity in the region.

Understanding post-glacial evolution of tidal dynamics also informs archaeo-ecological reconstructions. Past shoreline positions and sediment regimes can shape interpretations of human activity and ecosystem change. For example, changes in tidal amplitude affect intertidal zone extent, which can have implications for human foraging habitats and settlement patterns since the Holocene (Barnett et al., 2020).

4.3. Evolution of Shelf Sea Dynamics

Changes in ocean tides and relative sea levels since the LGM have fundamentally reorganized tidal dynamics across the Patagonian Shelf. These results demonstrate that even small sea-level changes can drive significant shifts in tidal dynamics, consistent with the findings of Carless et al. (2016) under future sea-level rise scenarios. M_2 and S_2 tidal elevation amplitudes increased as the shelf became progressively inundated, while diurnal constituents (K_1 and O_1) were generally higher in the past, particularly across the southern shelf. Present-day dissipation estimates for the shelf (148 GW, M_2 only) are broadly consistent with previous studies, including 128–153 GW reported by Carless et al. (2016), 95–138 GW by Egbert and Ray (2001), and 131 GW from the TPXO08 model (as cited in Carless et al., 2016). Variations between these absolute dissipation estimates reflect differences in model domains, shelf definitions, spatial resolution, numerical techniques, and input data sets such as bathymetry. Even a small overestimation of simulated tidal current speeds will inflate dissipation estimates, as tidal dissipation scales with the cube of tidal current speed (Section 2.3.3). Recent modeling of the present-day shelf by Dinápoli and Simionato (2024) reports an integrated tidal dissipation of 119 GW for eight constituents across the "Southwestern Atlantic Continental Shelf", lower than the value presented here. Their spatially-varying drag coefficient and assimilative methodology produce a present-day configuration optimized for accuracy, while our constant drag coefficient and palaeo-ocean boundary forcing are chosen to ensure consistency across 21 ka of palaeotidal simulations. These methodological differences affect absolute dissipation estimates, but do not undermine the validity of our estimates within a long-term shelf evolution context.

The value of the regional paleotidal model developed here lies in its applications - enabling interpretation of sea-level indicators, stratification patterns, and potential sediment transport and carbon accumulation processes that cannot be addressed using the coarser resolution global model. Understanding these processes is important because variations in tidal dynamics across the Patagonian Shelf have wide-ranging consequences. Indeed, the present-day shelf supports one of the most productive temperate marine ecosystems globally (Gil et al., 2019), and its shallow, biologically active waters suggest a significant role in organic carbon accumulation, particularly in the muddy depocenters of the inner shelf (Violante et al., 2014). As temperate shelf seas worldwide expanded with post-glacial sea-level rise, their role in atmosphere–ocean CO_2 exchange increased, with seasonal stratification playing a key role (Rippeth et al., 2008). The absence of a functioning "continental shelf pump" on the Patagonian Shelf (Bianchi et al., 2005), caused by shelf waters being less dense than the adjacent Malvinas Current, limits physical export of carbon to the deep ocean. However, this does not preclude the region from acting as a net CO_2 sink. Organic matter produced during seasonal phytoplankton blooms can settle to the seabed, where a fraction escapes remineralization and can accumulate in seabed sediments. Prior to ~8 ka BP, when the Patagonian Shelf was smaller, the region likely played a lesser role in global carbon cycling. From ~8 ka BP onwards, the present-day shelf configuration was largely established, with over 90% of the shelf seasonally stratified, potentially enhancing conditions for organic carbon accumulation in subtidal sediments. The model outputs presented here can be used to investigate organic carbon burial efficiency under varying past conditions, integrating geological observations with hydrodynamic modeling.

The Patagonian Shelf remains underexplored from a multidisciplinary perspective, with substantial data gaps in publicly available geological data and regional ocean model outputs. This work helps address these gaps through the first open-access, regional paleotidal model for the wider Patagonian Shelf. Previous work has been more spatially or temporally confined, including recent work by Alonso et al. (2025), who focused on the San Matías Gulf at 11.5 ka BP, using a two-dimensional M_2-only tidal model with 4 km horizontal resolution. Their methodology and results differ from ours in several ways. They used low-resolution present-day boundary forcing, a uniform 50 m sea-level drop, and ICE-4G-derived paleocoastlines, whereas our reconstructions are based on a new GIA model, indicating relative sea levels of ~45–35 m below present between 12 and 11 ka BP. A further difference between the modeling techniques is that Alonso et al. (2025) used nautical charts for bathymetry. Our GEBCO-derived bathymetry does not resolve a 60 m sill at the entrance of the Gulf (Isla, 2013), potentially leading to premature flooding in our simulations (soon after 14 ka BP); indeed observational data suggest the Gulf was not submerged until ~10 ka BP (Isla, 2013). These discrepancies highlight the need to reconcile model outputs with geological evidence and to assess the implications of different model input data sets.

Looking ahead, projected changes in sea level, ocean warming, and wind patterns are expected to alter tidal dynamics and seasonal stratification across global shelf seas (Carless et al., 2016; Haigh et al., 2020; Sharples et al., 2020; Shutler et al., 2025; Tinker et al., 2024). For example, Carless et al. (2016) showed that simulated tidal responses on the Patagonian Shelf are highly sensitive to how sea-level rise is implemented in models. Their simulations demonstrate that spatially varying sea-level trends produce different tidal outcomes compared to uniform scenarios. Notably, the M_2 constituent, near resonance at present, is especially sensitive to sea-level changes, suggesting that even modest sea-level rise could significantly alter tidal dynamics, with implications for coastal flood risk, sediment transport, ecosystem functioning, and carbon accumulation in subtidal sediments.

This highlights the value of both paleo- and future tidal modeling for informing climate adaptation strategies in shelf sea regions, as past tidal responses provide essential context for anticipating future change.

4.4. Limitations and Broader Research Potential

While paleotidal models offer valuable insights into past shelf dynamics, their accuracy depends heavily on the quality of input data, particularly paleobathymetric grids and tidal boundary conditions derived from GIA models. Crucially, the relative sea-level curves used to build the model presented here were not constrained using regional paleotidal outputs, simply because such a model did not previously exist. This highlights the iterative nature of paleo-modeling: our simulations help fill that gap, but also inherit uncertainties embedded in the input data sets.

The tidal simulations presented here are barotropic and do not account for tidal energy conversion. This simplification—though justifiable in the context of this study (Carless et al., 2016)—means vertical mixing processes are not explicitly modeled. A full three-dimensional hydrodynamic model would address these processes more comprehensively, but at significantly higher computational cost. For the scope of this study, the barotropic approach was efficient and sufficiently validated against available observations.

At the time of model development, the spatially varying drag coefficient method proposed by Dinápoli and Simionato (2024) was not yet available. We therefore adopted a spatially homogeneous drag coefficient, a common practice in shelf-scale modeling (e.g., Carless et al., 2016; Robins et al., 2015; Ward et al., 2016; Ward, Bradley, Roseby, et al., 2025). However, their findings show that incorporating spatial variability improves tidal amplitude validation—particularly for the S_2 constituent—at coastal stations. Future studies should consider implementing this refinement to enhance model accuracy.

Beyond sea-level index point calibration, paleotidal models have interdisciplinary potential across archeology, ecology, and climate science. In blue carbon research, these simulations can help identify periods and locations of enhanced fine sediment deposition, potentially linked to organic carbon accumulation driven by tidal dynamics. Tidal currents redistribute sediment across shelf scales, with parameters such as bed shear stress and bottom boundary layer thickness influencing depositional patterns and erosion rates (Ward et al., 2015; Ward, Bradley, Roseby, et al., 2025; Williams et al., 2019). These dynamics, combined with seasonal stratification, are likely to have shaped organic carbon burial over time. In poorly studied regions, like the Patagonian Shelf, model outputs could help identify priority regions for the study of shelf carbon stocks and their vulnerability to human disturbance and remineralization. Future work should assess burial efficiency under varying paleotidal conditions, integrating geological observations with model outputs to evaluate tidal influences on long-term carbon accumulation across the Patagonian Shelf.

5. Conclusions

This study presents the first paleotidal reconstruction for the wider Patagonian Shelf. By integrating new GIA modeling and refined global paleo-ocean forcing, our shelf-scale tidal simulations suggest that tidal dynamics across the Patagonian Shelf have undergone substantial spatial and temporal shifts since the LGM. These changes are primarily driven by changes in relative sea level and coastline evolution. Tidal energy dissipation across the shelf did not scale with shelf inundation but evolved non-linearly. M_2 dissipation dominated throughout deglaciation, peaking at 10 ka BP, despite the shelf being smaller than today, highlighting how shelf geometry can abruptly reorganize frictional hotspots, reshaping the mixing and transporting regimes across the shelf. Although shelf-scale O_1 dissipation has consistently been less than that of the semi-diurnal constituents, its variability since the LGM has been highly sensitive to deglacial shelf evolution. Our results help refine the indicative meaning of sea-level indicators, offering new constraints for interpreting sea-level index points in the region. The model outputs also challenge previous assumptions about paleogeographic connectivity, such as the isolation of the Islas Malvinas/Falkland Islands.

While the barotropic modeling approach used here is efficient and validated, future work should incorporate three-dimensional hydrodynamic simulations and explore tidal energy conversion processes to better resolve vertical mixing and internal tides. Further refinement of GIA models using regional tidal constraints will also be essential for improving sea-level reconstructions.

This work establishes a valuable baseline and provides new tools for interpreting coastal evolution, sea-level change, sediment transport, and organic carbon accumulation on the Patagonian Shelf, unlocking new directions for interdisciplinary research in this understudied region.

Conflict of Interest

The authors declare no conflicts of interest relevant to this study.

Availability Statement

The full suite of analyzed tidal model output, analysis scripts, glacial isostatic model output (relative sea level and ice sheet extent data sets) are available at Ward, Bradley, and Wilmes (2025).

Acknowledgments
The authors acknowledge funding from Convex Group Ltd for the Convex Seascape Survey, which is facilitated by Blue Marine Foundation (www.bluemarinefoundation.com/projects/convex-seascape-survey). The model simulations (of both SLW and SBW) were conducted on Supercomputing Wales, a collaboration between Welsh universities and the Welsh Government. The authors are grateful for ongoing technical support from Dr Ade Fewings and team (Digital Services, Bangor University).

References

Alonso, G., Dragani, W. C., & Isla, F. I. (2025). Reconstructing past tidal currents: A numerical approach to the paleotides of Northern Patagonia. *Estuarine, Coastal and Shelf Science*, *326*, 109536. https://doi.org/10.1016/j.ecss.2025.109536

Angulo, R. J., Lessa, G. C., & de Souza, M. C. (2006). A critical review of mid-to late-Holocene sea-level fluctuations on the eastern Brazilian coastline. *Quaternary Science Reviews*, *25*(5–6), 486–506. https://doi.org/10.1016/j.quascirev.2005.03.008

Austin, J. J., Soubrier, J., Prevosti, F. J., Prates, L., Trejo, V., Mena, F., & Cooper, A. (2013). The origins of the enigmatic Falkland Islands wolf. *Nature Communications*, *4*(1), 1552. https://doi.org/10.1038/ncomms2570

Barnett, R. L., Charman, D. J., Johns, C., Ward, S. L., Bevan, A., Bradley, S. L., et al. (2020). Nonlinear landscape and cultural response to sea-level rise. *Science Advances*, *6*(45), eabb6376. https://doi.org/10.1126/sciadv.abb6376

Bianchi, A. A., Bianucci, L., Piola, A. R., Pino, D. R., Schloss, I., Poisson, A., & Balestrini, C. F. (2005). Vertical stratification and air-sea CO_2 fluxes in the Patagonian shelf. *Journal of Geophysical Research*, *110*(C7). https://doi.org/10.1029/2004JC002488

Bini, M., Isola, I., Zanchetta, G., Pappalardo, M., Ribolini, A., Ragaini, L., et al. (2018). Mid-holocene relative sea-level changes along atlantic Patagonia: New data from Camarones, Chubut, Argentina. *The Holocene*, *28*(1), 56–64. https://doi.org/10.1177/0959683617714596

Bini, M., Zanchetta, G., Ribolini, A., Salvatore, M. C., Baroni, C., Pappalardo, M., et al. (2017). Last interglacial sea-level highstand deduced from notches and inner margins of marine terraces at Puerto Deseado, Santa Cruz Province, Argentina. *Geografia Fisica e Dinamica Quaternaria*, *40*. https://doi.org/10.4461/GFDQ2017.40.3

Bowers, D. G., & Simpson, J. H. (1987). Mean position of tidal fronts in european-shelf seas. *Continental Shelf Research*, *7*(1), 35–44. https://doi.org/10.1016/0278-4343(87)90062-8

Bradley, S. L., Milne, G. A., Horton, B. P., & Zong, Y. (2016). Modelling sea level data from China and Malay-Thailand to estimate Holocene ice volume equivalent sea level change. *Quaternary Science Reviews*, *137*, 54–68. https://doi.org/10.1016/j.quascirev.2016.02.002

Bradley, S. L., Milne, G. A., Shennan, I., & Edwards, R. (2011). An improved glacial isostatic adjustment model for the British Isles. *Journal of Quaternary Science*, *26*(5), 541–552. https://doi.org/10.1002/jqs.1481

Carless, S. J., Green, J. M., Pelling, H. E., & Wilmes, S. B. (2016). Effects of future sea-level rise on tidal processes on the Patagonian Shelf. *Journal of Marine Systems*, *163*, 113–124. https://doi.org/10.1016/j.jmarsys.2016.07.007

Chavez, F. P., Messié, M., & Pennington, J. T. (2011). Marine primary production in relation to climate variability and change. *Annual Review of Marine Science*, *3*(1), 227–260. https://doi.org/10.1146/annurev.marine.010908.163917

Clark, P. U., Dyke, A. S., Shakun, J. D., Carlson, A. E., Clark, J., Wohlfarth, B., et al. (2009). The last glacial maximum. *Science*, *325*(5941), 710–714. https://doi.org/10.1126/science.1172873

Combes, V., & Matano, R. P. (2018). The Patagonian shelf circulation: Drivers and variability. *Progress in Oceanography*, *167*, 24–43. https://doi.org/10.1016/j.pocean.2018.07.003

Darvill, C. M., Stokes, C. R., Bentley, M. J., Evans, D. J., & Lovell, H. (2016). Dynamics of former ice lobes of the southernmost Patagonian Ice Sheet based on a glacial landsystems approach. *Journal of Quaternary Science*, *32*(6), 857–876. https://doi.org/10.1002/jqs.2890

De Groeve, J., Kusumoto, B., Koene, E., Kissling, W. D., Seijmonsbergen, A. C., Hoeksema, B. W., et al. (2022). Global raster dataset on historical coastline positions and shelf sea extents since the last Glacial Maximum. *Global Ecology and Biogeography*, *31*(11), 2162–2171. https://doi.org/10.1111/geb.13573

Dinápoli, M. G., & Simionato, C. G. (2024). Study of the tidal dynamics in the Southwestern Atlantic Continental Shelf based on data assimilation. *Ocean Modelling*, *188*, 102332. https://doi.org/10.1016/j.ocemod.2024.102332

Dinápoli, M. G., & Simionato, C. G. (2025). On the magnitude and mechanisms of occurrence of nonlinear tide-surge interactions in the Southwestern Atlantic Continental Shelf. *Estuarine, Coastal and Shelf Science*, *323*, 109357. https://doi.org/10.1016/j.ecss.2025.109357

Dinápoli, M. G., Simionato, C. G., Alonso, G., Bodnariuk, N., & Saurral, R. (2024). Negative storm surges in the Río de la Plata Estuary: Mechanisms, variability, trends and linkage with the Continental Shelf dynamics. *Estuarine, Coastal and Shelf Science*, *305*, 108844. https://doi.org/10.1016/j.ecss.2024.108844

Dinápoli, M. G., Simionato, C. G., & Moreira, D. (2020). Nonlinear tide-surge interactions in the Río de la Plata Estuary. *Estuarine, Coastal and Shelf Science*, *241*, 106834. https://doi.org/10.1016/j.ecss.2020.106834

Egbert, G. D., & Erofeeva, S. Y. (2002). Efficient inverse modeling of barotropic ocean tides. *Journal of Atmospheric and Oceanic Technology*, *19*(2), 183–204. https://doi.org/10.1175/1520-0426(2002)019<0183:EIMOBO>2.0.CO;2

Egbert, G. D., & Ray, R. D. (2001). Estimates of M2 tidal energy dissipation from TOPEX/Poseidon altimeter data. *Journal of Geophysical Research*, *106*(C10), 22475–22502. https://doi.org/10.1029/2000JC000699

Egbert, G. D., Ray, R. D., & Bills, B. G. (2004). Numerical modeling of the global semidiurnal tide in the present day and in the last Glacial Maximum. *Journal of Geophysical Research*, *109*(C3). https://doi.org/10.1029/2003JC001973

Falkowski, P. G., Barber, R. T., & Smetacek, V. (1998). Biogeochemical controls and feedbacks on ocean primary production. *Science*, *281*(5374), 200–206. https://doi.org/10.1126/science.281.5374.200

Garrett, E., Melnick, M., Dura, T., Cisternas, M., Ely, L. L., Robert, L., et al. (2020). Holocene relative sea-level change along the tectonically active Chilean coast. *Quaternary Science Reviews*, *236*, 106281. https://doi.org/10.1016/j.quascirev.2020.106281

Gebbie, G. (2020). Cancelation of deglacial thermosteric Sea level rise by a barosteric effect. *Journal of Physical Oceanography*, *50*(12), 3623–3639. https://doi.org/10.1175/JPO-D-20-0173.1

GEBCO Compilation Group. (2023). GEBCO 2023 grid. https://doi.org/10.5285/f98b053b-0cbc-6c23-e053-6c86abc0af7b

GEF LME:LEARN. (2017). The large marine ecosystem approach: An engine for achieving SDG 14.

Gil, M. N., Giarratano, E., Barros, V., Bortolus, A., Codignotto, J. O., Schenke, R. D., et al. (2019). Southern Argentina: The patagonian continental shelf. In *World seas: An environmental evaluation* (pp. 783–811). Academic Press.

Glorioso, P. D. (2000). Patagonian shelf 3D tide and surge model. *Journal of Marine Systems*, *24*(1–2), 141–151. https://doi.org/10.1016/S0924-7963(99)00084-6

Glorioso, P. D., & Flather, R. A. (1995). A barotropic model of the currents off SE South America. *Journal of Geophysical Research*, *100*(C7), 13427–13440. https://doi.org/10.1029/95JC00942

Glorioso, P. D., & Flather, R. A. (1997). The Patagonian shelf tides. *Progress in Oceanography*, *40*(1–4), 263–283. https://doi.org/10.1016/S0079-6611(98)00004-4

Glorioso, P. D., & Simpson, J. H. (1994). Numerical modelling of the M2 tide on the northern Patagonian Shelf. *Continental Shelf Research*, *14*(2–3), 267–278. https://doi.org/10.1016/0278-4343(94)90016-7

Gowan, E. J., Tregoning, P., Purcell, A., Lea, J., Fransner, O. J., Noormets, R., & Dowdeswell, J. A. (2016). Icesheet 1.0: A program to produce paleo-ice sheet reconstructions with minimal assumptions. *Geoscientific Model Development*, *9*(5), 1673–1682. https://doi.org/10.5194/gmd-9-1673-2016

Gowan, E. J., Zhang, X., Khosravi, S., Rovere, A., Stocchi, P., Hughes, A. L. C., et al. (2021). A new global ice sheet reconstruction for the past 80 000 years. *Nature Communications*, *12*(1), 1199. https://doi.org/10.1038/s41467-021-21469-w

Green, J. A. M. (2010). Ocean tides and resonance. *Ocean Dynamics*, *60*(5), 1243–1253. https://doi.org/10.1007/s10236-010-0331-1

Green, J. A. M., & Nycander, J. (2013). A comparison of internal wavedrag parameterizations for tidal models. *Journal of Physical Oceanography*, *43*(1), 104–119. https://doi.org/10.1175/JPO-D-12-023.1

Gregory, J. M., Griffies, S. M., Hughes, C. W., Lowe, J. A., Church, J. A., Fukimori, I., et al. (2019). Concepts and terminology for sea level: Mean, variability and change, both local and global. *Surveys in Geophysics*, *40*(6), 1251–1289. https://doi.org/10.1007/s10712-019-09525-z

Guilderson, T. P., Burckle, L., Hemming, S., & Peltier, W. R. (2000). Late Pleistocene sea level variations derived from the Argentine Shelf. *Geochemistry, Geophysics, Geosystems*, *1*(12). https://doi.org/10.1029/2000GC000098

Guo, L., Brand, M., Sanders, B. F., Foufoula-Georgiou, E., & Stein, E. D. (2018). Tidal asymmetry and residual sediment transport in a short tidal basin under sea level rise. *Advances in Water Resources*, *121*, 1–8. https://doi.org/10.1016/j.advwatres.2018.07.012

Gyllencreutz, R., Mahiques, M. M. D., Alves, D. V. P., & Wainer, I. K. C. (2010). Mid-to late-holocene paleoceanographic changes on the southeastern Brazilian shelf based on grain size records. *The Holocene*, *20*(6), 863–875. https://doi.org/10.1177/0959683610365936

Haigh, I. D., Pickering, M. D., Green, J. M., Arbic, B. K., Arns, A., Dangendorf, S., et al. (2020). The tides they are a-Changin': A comprehensive review of past and future nonastronomical changes in tides, their driving mechanisms, and future implications. *Reviews of Geophysics*, *58*(1), e2018RG000636. https://doi.org/10.1029/2018RG000636

Hall, P., & Davies, A. M. (2004). Modelling tidally induced sediment-transport paths over the northwest European shelf: The influence of sea-level reduction. *Ocean Dynamics*, *54*(2), 126–141. https://doi.org/10.1007/s10236-003-0070-7

Hamley, K. M., Gill, J. L., Krasinski, K. E., Groff, D. V., Hall, B. L., Sandweiss, D. H., et al. (2021). Evidence of prehistoric human activity in the Falkland Islands. *Science Advances*, *7*(44), eabh3803. https://doi.org/10.1126/sciadv.abh3803

Hayden, A. M., Wilmes, S. B., Gomez, N., Green, J. A. M., Pan, L., Han, H., & Golledge, N. R. (2020). Multi-Century impacts of ice sheet retreat on Sea level and Ocean tides in Hudson Bay. *Journal of Geophysical Research: Oceans*, *125*(11), e2019JC015104. https://doi.org/10.1029/2019JC015104

Hendershott, M. C. (1972). Numerical models of ocean tides. *Sea*, *6*, 47–95.

Hervouet, J. M. (2000). TELEMAC modelling system: An overview. *Hydrological Processes*, *14*(13), 2209–2210. https://doi.org/10.1002/1099-1085(200009)14:13<2209::AID-HYP23>3.0.CO;2-6

Hill, D. F. (2016). Spatial and temporal variability in tidal range: Evidence, causes, and effects. *Current Climate Change Reports*, *2*(4), 232–241. https://doi.org/10.1007/s40641-016-0044-8

Hinton, A. C. (1996). Tides in the northeast Atlantic: Considerations for modelling water depth changes. *Quaternary Science Reviews*, *15*(8–9), 873–894. https://doi.org/10.1016/S0277-3791(96)00061-3

Isla, F. I. (2013). The flooding of the San Matías Gulf: The Northern Patagonia sea-level curve. *Geomorphology*, *203*, 60–65. https://doi.org/10.1016/j.geomorph.2013.02.013

Kendall, R. A., Mitrovica, J. X., & Milne, G. A. (2005). On post-glacial sea level – II. Numerical formulation and comparative results on spherically symmetric models. *Geophysical Journal International*, *161*(3), 679–706. https://doi.org/10.1111/j.1365-246X.2005.02553.x

Ladant, J. B., Millot-Weil, J., de Lavergne, C., Green, J. M., Nguyen, S., & Donnadieu, Y. (2024). The role of tidal mixing in shaping early Eocene deep ocean circulation and oxygenation. *Paleoceanography and Paleoclimatology*, *39*(7), e2023PA004822. https://doi.org/10.1029/2023PA004822

Lambeck, K., Rouby, H., Purcell, A., Sun, Y., & Sambridge, M. (2014). Sea level and global ice volumes from the Last Glacial Maximum to the Holocene. *Proceedings of the National Academy of Sciences*, *111*(43), 15296–15303. https://doi.org/10.1073/pnas.1411762111

Lange, H., Casassa, G., Ivins, E. R., Schroder, L., Fritsche, M., Richter, A., et al. (2014). Observed crustal uplift near the Southern Patagonian Icefield constrains improved viscoelastic Earth models. *Geophysical Research Letters*, *41*(3), 805–812. https://doi.org/10.1002/2013GL058419

Leorri, E., Mulligan, R., Mallinson, D., & Cearreta, A. (2011). Sea-level rise and local tidal range changes in coastal embayments: An added complexity in developing reliable sea-level index points. *Revista de Gestão Costeira Integrada – Journal of Integrated Coastal Zone Management*, *11*(3), 307–314. https://doi.org/10.5894/rgci277

Lowry, D. P., Han, H. K., Golledge, N. R., Gomez, N., Johnson, K. M., & McKay, R. M. (2024). Ocean cavity regime shift reversed West Antarctic grounding line retreat in the late Holocene. *Nature Communications*, *15*(1), 3176. https://doi.org/10.1038/s41467-024-47369-3

Luz Clara, M., Simionato, C. G., D'Onofrio, E., & Moreira, D. (2015). Future sea level rise and changes on tides in the Patagonian Continental Shelf. *Journal of Coastal Research*, *31*(3), 519–535. https://doi.org/10.2112/JCOASTRES-D-13-00127.1

Melet, A. V., Hallberg, R., & Marshall, D. P. (2022). Chapter 2 – The role of ocean mixing in the climate system. In M. Meredith & A. Naveira Garabato (Eds.), *Ocean mixing* (pp. 5–34). Elsevier.

Milne, G. A., Long, A. J., & Bassett, S. E. (2005). Modelling Holocene relative sea-level observations from the Caribbean and South America. *Quaternary Science Reviews*, *24*(10–11), 1183–1202. https://doi.org/10.1016/j.quascirev.2004.10.005

Mitrovica, J. X., & Milne, G. A. (2003). On post-glacial sea level: I. General theory. *Geophysical Journal International*, *154*(2), 253–267. https://doi.org/10.1046/j.1365-246X.2003.01942.x

Moreira, D., Simionato, C. G., & Dragani, W. (2011). Modeling ocean tides and their energetics in the North Patagonia Gulfs of Argentina. *Journal of Coastal Research*, *27*(1), 87–102. https://doi.org/10.2112/JCOASTRES-D-09-00055
Müller, M., Arbic, B. K., & Mitrovica, J. X. (2011). Secular trends in ocean tides: Observations and model results. *Journal of Geophysical Research*, *116*(C5), C05013. https://doi.org/10.1029/2010JC006387
Munk, W. (1997). Once again: Once again—tidal friction. *Progress in Oceanography*, *40*(1–4), 7–35. https://doi.org/10.1016/S0079-6611(97)00021-9
Neill, S. P., Scourse, J. D., & Uehara, K. (2010). Evolution of bed shear stress distribution over the northwest European shelf seas during the last 12,000 years. *Ocean Dynamics*, *60*(5), 1139–1156. https://doi.org/10.1007/s10236-010-0313-3
Palma, E. D., Matano, R. P., & Piola, A. R. (2004). A numerical study of the Southwestern Atlantic Shelf circulation: Barotropic response to tidal and wind forcing. *Journal of Geophysical Research*, *109*(C8). https://doi.org/10.1029/2004JC002315
Palma, E. D., Matano, R. P., & Piola, A. R. (2008). A numerical study of the Southwestern Atlantic Shelf circulation: Stratified ocean response to local and offshore forcing. *Journal of Geophysical Research*, *113*(C11). https://doi.org/10.1029/2007JC004720
Pappalardo, M., Baroni, C., Bini, M., Isola, I., Ribolini, A., Salvatore, M. C., & Zanchetta, G. (2019). Challenges in relative sea-level change assessment highlighted through a case study: The central coast of Atlantic Patagonia. *Global and Planetary Change*, *182*, 103008. https://doi.org/10.1127/0372-8854/2014/0142
Pawlowicz, R., Beardsley, R. C., & Lentz, S. J. (2002). Classical tidal harmonic analysis including error estimates in MATLAB. *Ocean Modelling*, *5*(3), 371–380. https://doi.org/10.1016/s1463-5003(02)00003-8
Peltier, W. R. (2002). On eustatic sea level history: Last Glacial Maximum to Holocene. *Quaternary Science Reviews*, *21*(1–3), 377–396. https://doi.org/10.1016/S0277-3791(01)00084-1
Piccioni, G., Dettmering, D., Bosch, W., & Seitz, F. (2019). Ticon: TIdal CONstants based on GESLA sea-level records from globally located tide gauges. *Geoscience Data Journal*, *6*(2), 97–104. https://doi.org/10.1002/gdj3.72
Ponce, J. F., Rabassa, J., Coronato, A., & Borromei, A. M. (2011). Palaeogeographical evolution of the Atlantic coast of Pampa and Patagonia from the last glacial maximum to the Middle Holocene. *Biological Journal of the Linnean Society*, *103*(2), 363–379. https://doi.org/10.1111/j.1095-8312.2011.01653.x
Pugh, D., & Woodworth, P. (2014). *Sea-level science: Understanding tides, surges, tsunamis and mean sea-level changes*. Cambridge University Press.
Rippeth, T. P., Scourse, J. D., Uehara, K., & McKeown, S. (2008). Impact of sea-level rise over the last deglacial transition on the strength of the continental shelf CO_2 pump. *Geophysical Research Letters*, *35*(24). https://doi.org/10.1029/2008GL035880
Robins, P. E., Neill, S. P., Lewis, M. J., & Ward, S. L. (2015). Characterising the spatial and temporal variability of the tidal-stream energy resource over the northwest European shelf seas. *Applied Energy*, *147*, 510–522. https://doi.org/10.1016/j.apenergy.2015.03.045
Ruiz Etcheverry, L. A., Saraceno, M., Piola, A. R., & Strub, P. T. (2016). Sea level anomaly on the Patagonian continental shelf: Trends, annual patterns and geostrophic flows. *Journal of Geophysical Research: Oceans*, *121*(4), 2733–2754. https://doi.org/10.1002/2015JC011265
Schaffer, J., Timmermann, R., Arndt, J. E., Kristensen, S. S., Mayer, C., Morlighem, M., & Steinhage, D. (2016). A global, high-resolution data set of ice sheet topography, cavity geometry, and ocean bathymetry. *Earth System Science Data*, *8*(2), 543–557. https://doi.org/10.5194/essd-8-543-2016
Schellmann, G., & Radtke, U. (2010). Timing and magnitude of Holocene sea-level changes along the middle and south Patagonian Atlantic coast derived from beach ridge systems, littoral terraces and valley-mouth terraces. *Earth-Science Reviews*, *103*(1–2), 1–30. https://doi.org/10.1016/j.earscirev.2010.06.003
Schindelegger, M., Green, J. A. M., Wilmes, S. B., & Haigh, I. D. (2018). Can we model the effect of observed sea level rise on tides? *Journal of Geophysical Research: Oceans*, *123*(7), 4593–4609. https://doi.org/10.1029/2018jc013959
Schmittner, A., Green, J. A. M., & Wilmes, S. B. (2015). Glacial ocean overturning intensified by tidal mixing in a global circulation model. *Geophysical Research Letters*, *42*(10), 4014–4022. https://doi.org/10.1002/2015GL06356
Scourse, J., Uehara, K., & Wainwright, A. (2009). Celtic Sea linear tidal sand ridges, the Irish Sea Ice Stream and the Fleuve Manche: Palaeotidal modelling of a transitional passive margin depositional system. *Marine Geology*, *259*(1–4), 102–111. https://doi.org/10.1016/j.margeo.2008.12.010
Scourse, J. D. (2013). Quaternary sea level and palaeotidal changes: A review of impacts on, and responses of, the marine biosphere. *Oceanography and Marine Biology an Annual Review*, *51*, 1–70. https://doi.org/10.1201/b15406
Scourse, J. D., Austin, W. E. N., Long, B. T., Assinder, D. J., & Huws, D. (2002). Holocene evolution of seasonal stratification in the Celtic Sea: Refined age model, mixing depths and foraminiferal stratigraphy. *Marine Geology*, *191*(3–4), 119–145. https://doi.org/10.1016/S0025-3227(02)00528-5
Sharples, J., Holt, J., & Wakelin, S. (2020). Impacts of climate change on shelf sea stratification, relevant to the coastal and marine environment around the UK. *MCCIP Science Review*, *2020*, 103–115. https://doi.org/10.14465/2020.arc05.str
Shutler, J. D., Ford, D. J., Holding, T., Ubelmann, C., Gaultier, L., Collard, F., et al. (2025). Wind-driven control of shelf-sea CO2 sinks. *Global Biogeochemical Cycles*, *39*(9), e2024GB008461. https://doi.org/10.1029/2024GB008461
Simionato, C. G., Dragani, W., Nuñez, M., & Engel, M. (2004). A set of 3-D nested models for tidal propagation from the Argentinean continental shelf to the Río de la Plata estuary—Part I. M2. *Journal of Coastal Research*, *20*(3), 893–912. https://doi.org/10.2112/1551-5036(2004)20[893:ASODNM]2.0.CO;2
Simpson, J. H., & Hunter, J. R. (1974). Fronts in the Irish sea. *Nature*, *250*(5465), 404–406. https://doi.org/10.1038/250404a0
Sulzbach, R., Klemann, V., Knorr, G., Dobslaw, H., Dümpelmann, H., Lohmann, G., & Thomas, M. (2023). Evolution of global ocean tide levels since the last Glacial Maximum. *Paleoceanography and Paleoclimatology*, *38*(5), e2022PA004556. https://doi.org/10.1029/2022PA004556
Taylor, G. I. (1920). Tidal friction in the Irish Sea. *Philosophical Transactions of the Royal Society of London A*, *230*, 1–93. https://doi.org/10.1098/rsta.1920.0001
Thomas, H., Bozec, Y., Elkalay, K., & De Baar, H. J. (2004). Enhanced open ocean storage of CO2 from shelf sea pumping. *Science*, *304*(5673), 1005–1008. https://doi.org/10.1126/science.1095491
Tinker, J., Palmer, M. D., Harrison, B. J., O'Dea, E., Sexton, D. M., Yamazaki, K., & Rostron, J. W. (2024). Twenty-first century marine climate projections for the NW European shelf seas based on a perturbed parameter ensemble. *Ocean Science*, *20*(3), 835–885. https://doi.org/10.5194/os-20-835-2024
Uehara, K., Scourse, J. D., Horsburgh, K. J., Lambeck, K., & Purcell, A. P. (2006). Tidal evolution of the northwest European shelf seas from the Last Glacial Maximum to the present. *Journal of Geophysical Research*, *111*(C9). https://doi.org/10.1029/2006JC003531
Van der Molen, J., & De Swart, H. E. (2001). Holocene tidal conditions and tide-induced sand transport in the southern North Sea. *Journal of Geophysical Research*, *106*(C5), 9339–9362. https://doi.org/10.1029/2000JC000488

Violante, R. A. (2005). Submerged terraces in the continental shelf of Argentina and its significance as paleo-sea level indicators: The example of the Rioplatense Terrace. *5th Annual Conference Project IGCP*, *464*, 97–99.
Violante, R. A., & Parker, G. (2004). The post-last glacial maximum transgression in the de la Plata River and adjacent inner continental shelf, Argentina. *Quaternary International*, *114*(1), 167–181. https://doi.org/10.1016/S1040-6182(03)00036-3
Violante, R. A., Paterlini, C. M., Marcolini, S. I., Costa, I. P., Cavallotto, J. L., Laprida, C., et al. (2014). The Argentine continental shelf: Morphology, sediments, processes and evolution since the last Glacial Maximum. *Geological Society, London, Memoirs*, *41*(1), 55–68. https://doi.org/10.1144/m41.6
Ward, S., Bradley, S. L., & Wilmes, S.-B. (2025). Relative sea-level change, tidal evolution and energy dissipation across the Patagonian continental shelf since the last Glacial Maximum [Dataset]. *Zenodo*. https://doi.org/10.5281/zenodo.17724428
Ward, S. L., Bradley, S. L., Roseby, Z. A., Wilmes, S. B., Vosper, D. F., Roberts, C. M., & Scourse, J. D. (2025). The role of long-term hydrodynamic evolution in the accumulation and preservation of organic carbon-rich shelf sea deposits. *Journal of Geophysical Research: Oceans*, *130*(4), e2024JC022092. https://doi.org/10.1029/2024JC022092
Ward, S. L., Green, J. M., & Pelling, H. E. (2012). Tides, sea-level rise and tidal power extraction on the European shelf. *Ocean Dynamics*, *62*(8), 1153–1167. https://doi.org/10.1007/s10236-012-0552-6
Ward, S. L., Neill, S. P., Scourse, J. D., Bradley, S. L., & Uehara, K. (2016). Sensitivity of palaeotidal models of the northwest European shelf seas to glacial isostatic adjustment since the last Glacial Maximum. *Quaternary Science Reviews*, *151*, 198–211. https://doi.org/10.1016/j.quascirev.2016.08.034
Ward, S. L., Neill, S. P., Van Landeghem, K. J., & Scourse, J. D. (2015). Classifying seabed sediment type using simulated tidal-induced bed shear stress. *Marine Geology*, *367*, 94–104. https://doi.org/10.1016/j.margeo.2015.05.010
Weatherall, P., Marks, K. M., Jakobsson, M., Schmitt, T., Tani, S., Arndt, J. E., et al. (2015). A new digital bathymetric model of the world's oceans. *Earth and Space Science*, *2*, 331–345. https://doi.org/10.1002/2015EA000107
Webb, D. J. (1976). A model of continental-shelf resonances. *Deep-Sea Research and Oceanographic Abstracts*, *23*(1), 1–15. https://doi.org/10.1016/0011-7471(76)90804-4
Williams, M. E., Amoudry, L. O., Brown, J. M., & Thompson, C. E. L. (2019). Fine particle retention and deposition in regions of cyclonic tidal current rotation. *Marine Geology*, *410*, 122–134. https://doi.org/10.1016/j.margeo.2019.01.006
Wilmes, S. B., & Green, J. A. M. (2014). The evolution of tides and tidal dissipation over the past 21,000 years. *Journal of Geophysical Research: Oceans*, *119*(7), 4083–4100. https://doi.org/10.1002/2013JC009605
Wilmes, S. B., Pedersen, V. K., Schindelegger, M., & Green, J. A. M. (2023). Late Pleistocene evolution of tides and tidal dissipation. *Paleoceanography and Paleoclimatology*, *38*(11), e2023PA004727. https://doi.org/10.1029/2023PA004727
Woods, M. A., Wilkinson, I. P., Leng, M. J., Riding, J. B., Vane, C. H., dos Santos, R. A. L., et al. (2019). Tracking Holocene palaeostratification and productivity changes in the Western Irish Sea: A multi-proxy record. *Palaeogeography, Palaeoclimatology, Palaeoecology*, *532*, 109231. https://doi.org/10.1016/j.palaeo.2019.06.004
Zaron, E. D., & Egbert, G. D. (2006). Estimating open-ocean barotropic tidal dissipation: The Hawaiian Ridge. *Journal of Physical Oceanography*, *36*(6), 1019–1035. https://doi.org/10.1175/JPO2878.1